

Internal Report  
Fermilab Report No. 77-89  
Lehigh Univ. Report No. LEH-24  
Univ. of Pa. Report No. UPR-0024E  
Univ. of Wis. Report No. C00/0081-4

10-3-77; Preliminary Version

EVIDENCE FOR JETS, AND FOR CORRELATED JETS,

IN HIGH  $P_T$  EVENTS \*

L. Cornell, M. Corcoran, M. Dris, A. Erwin, P. Gollon, E. Harvey, A. Kanofsky  
W. Kononenko, G. Lazo, R. Loveless, E. M. O'Neill, B. Robinson, W. Selove,  
M. Thompson, B. Yost, J. Bednar, C. Cortez, T. Duesing, D. Holler, R. Manulik

---

Fermilab-Lehigh-University of Pennsylvania-University of Wisconsin

\* Work supported by the U.S. Energy Research and Development Administration

EVIDENCE FOR JETS, AND FOR CORRELATED JETS,

IN HIGH  $P_T$  EVENTS

L. Cornell, M. Corcoran, M. Dris, A. Erwin, P. Gollon, E. Harvey, A. Kanofsky, W. Kononenko, G. Lazo, R. Loveless, E. M. O'Neill, B. Robinson, W. Selove, M. Thompson, B. Yost, J. Bednar, C. Cortez, T. Duesing, D. Holler, R. Manulik

---

Fermilab, Batavia, Ill.; Lehigh University, Bethlehem, Pa.; Univ. of Pennsylvania, Philadelphia, Pa.; and Univ. of Wisconsin, Madison, Wis.

---

ABSTRACT: A two-arm calorimeter array has been used to study events of high  $p_T$ , using 200 GeV and 400 GeV beams at Fermilab. The two arms, not identical, cover about 1.5 sr each, roughly centered near  $90^\circ$  CM on each side of the beam.

New results are found, particularly on three subjects. (1) The structure of the high  $p_T$  groups is characteristic of what has been predicted for "jets". (2) High total  $p_T$  in one arm is accompanied in general by high  $p_T$  in the other arm. The "away" side  $p_T$  spectrum in fact shows a peak. The position of that peak tends to increase with increasing trigger-side  $p_T$ . (3) A two-arm-sum trigger was also used. This trigger shows evidence of a strongly correlated two-jet structure for the high  $p_T$  events, and also gives information on the magnitude of the quark/parton transverse momentum in a parton scattering model.

CONTENTS

1. Introduction, and summary of principal results.
2. Apparatus
3. Triggering arrangement
4. Background
5. Character of multiple particle and single particle events
6. The "jet axis", and the  $\cos \alpha$  distribution
7. Relative rates of multiple particle and single particle events at high  $p_T$ .
8. Are the events "jet"-like in the form predicted by Bjorken et al?
9. Cross section for jets
10. Observation of a peak in the away-side  $P_T$  distribution. Transverse momentum of quarks/partons.
11. The L+R trigger. Two-jet correlations. Quark/parton transverse momentum.
12. Comparison of jets produced by  $\pi^+$  and proton beams.
13. Acknowledgments.

## 1. INTRODUCTION AND SUMMARY

This is a report on the first results from a new high  $p_T$  experiment still in progress.

The study of high  $p_T$  events in hadron-hadron interactions has been pursued intensively in recent years, with the particular hope of seeing a relatively simple basic character to those events at sufficiently high  $p_T$ , a "jet"-like character, which could hopefully give information on the scattering of quarks or partons, and thus perhaps on the forces between them. The first suggestion that such jets might occur, and might be produced in the scatterings of hadron constituents, was made by Berman Bjorken and Kogut (BBK)<sup>(1)</sup>; the subject was further developed by Bjorken<sup>(2)</sup> and by other authors<sup>(3)</sup>. Some important recent results are described in papers by Darriulat et al<sup>(4)</sup>, by Della Negra et al<sup>(5)</sup>, by Jacob<sup>(6)</sup>, and particularly by Bromberg et al<sup>(7,8)</sup>. The recent theoretical literature on this subject, like the experimental, is voluminous-- we mention particularly recent papers by Feynman and his collaborators<sup>(9,10)</sup> by Landshoff<sup>(11)</sup>, and by Ellis and Stroynowski<sup>(12)</sup>; a further very extensive list can be found in reference 3.

The recent experimental results, as described in references 4-8, have given increasing confirmation of some of the predictions of the BBK model. We report here the first results from a new high  $p_T$  experiment, which bear on the existence and character of jets, and on associated phenomena.

From an extensive preliminary analysis of the data obtained so far, mostly in about 100 hours of data taking under various beam and geometry conditions, we have found the following principal results.

- 1) High  $p_T$  events of 3 to 6 GeV/c total  $p_T$ , detected in a  $1\frac{1}{2}$  sr calorimeter detector located near  $90^\circ$  CM, occur much more frequently as clustered groups of particles relatively close together than as single particle events.
- 2) The clustering grows tighter, in terms of  $\Delta p_T / \Delta \Omega$ , as  $p_T$  (total) grows larger. At the upper end of our  $p_T$  range, 5 GeV/c or so, the typical

multiplicity in the calorimeter is about 5 or 6. Typically, at this total  $p_T$ , one sees a "core", with 3 particles or so each of  $p_T$  above 1 GeV/c, all 3 lying in a  $\Delta\Omega$  of about 1/2 steradian. In the additional 2 sr or so surrounding the calorimeter we see evidence, from the drift chamber information, that only 2 or 3 additional particles occur, compared to the 5 or 6 which are more tightly clustered in the calorimeter.

These characteristics, together, correspond to those which have been predicted for "jets". By a jet we shall mean a multi-particle group with such a high value of  $\Delta p_T / \Delta\Omega$  that kinematically it stands clearly distinct from any surrounding high  $p_T$  particles or groups. Clearly if 40 to 45% of the total initial beam energy,  $\frac{1}{2}\sqrt{s}$ , goes as a multiparticle group into a 1/2 sr region, one cannot have many other such concentrations of  $\Delta p_T / \Delta\Omega$  present in that event.

- 3) When one triggers on events with some high  $p_T$  band in one arm, the "away" side total  $p_T$ , in a calorimeter detector of 1 to  $1\frac{1}{2}$  sr, shows a peak in  $p_T(\text{away})$ .

This is a new result. The presence of this away-side peak, and its detailed characteristics, discussed below, give evidence of a correlated two-jet structure in high  $p_T$  events (i.e., two large-angle jets), and suggest that one is seeing hard collisions between hadron constituents.

- 4) We have also used a trigger which sums the two arm  $p_T$  magnitudes ("L+R" trigger). This trigger is free of the trigger bias expected to result, in single-arm triggering, from initial transverse momentum of the partons<sup>(5,6,10,12)</sup>. The results (a) show further strong evidence of correlated two-jet structure, and (b) give a further indication, beyond other methods used previously, that the initial transverse momentum of the colliding constituents is about 3/4 GeV/c, in the events studied so far.

- 5) We have also studied the ratio,

$$R \equiv \frac{\sigma_{(pp) \rightarrow \text{jet} + x}}{\sigma_{(\pi^+ p) \rightarrow \text{jet} + x}}$$

for a 200 GeV beam. As  $p_T(\text{jet})$  increases from 1.5 to 5 GeV/c, R decreases from about 1.5 to about 3/4.

## 2. APPARATUS

The apparatus consisted of a two arm segmented calorimeter array, with 6 planes of drift chambers between the hydrogen target and the calorimeter system. The calorimeter array was readily movable along the beam direction, and was operated at two different positions in the data reported here. In both cases, the solid angle covered by each arm was about  $1\frac{1}{2}$  sr(CM).

Figure 1 shows a schematic top view of the apparatus, in the "7 meter" position. Data at 400 GeV were principally taken in this position. The calorimeter was also operated in a "4 meter" position, where the 200 GeV data reported here were taken. All of the data described here were taken at 400 GeV, 7 m position, unless otherwise stated.

The calorimeter was of modular construction, segmented in area (into "segments") and in depth. The Right (R) arm has 25 segments; its construction is shown schematically in Figure 2. This figure shows an array of 25 segments, each segment 4 modules deep. The A, B, and C layers consist of steel-scintillator sandwiches, each module about 2 absorption lengths thick. The A' modules consist of thin (3 layer) lead-scintillator sandwiches, and have the purpose of providing a quite clear distinction between  $\pi^0$ 's and other hadrons--this is important since the pulse height of purely electromagnetic showers is substantially higher, for a given incident energy, than the most probable pulse height of non-e-m showers. As described below, the A' modules, together with the depth segmenting of the calorimeter system, give a very clear separation of e-m and non-e-m showers, when there is no more than one particle entering a given segment.

The modules in the Right arm are of two different cross sections, 15 cm x 15 cm and 20 x 20. The modules are arranged with the size stepping from the smaller size to the larger one both horizontally and in depth, to optimize solid angle subdivision and to make each segment "aim" reasonably well at the target. This is shown further, schematically, below.

The calorimeter modules indicated in Figure 2 use a fluorescent bar light collection technique developed by us, and described schematically in a previous

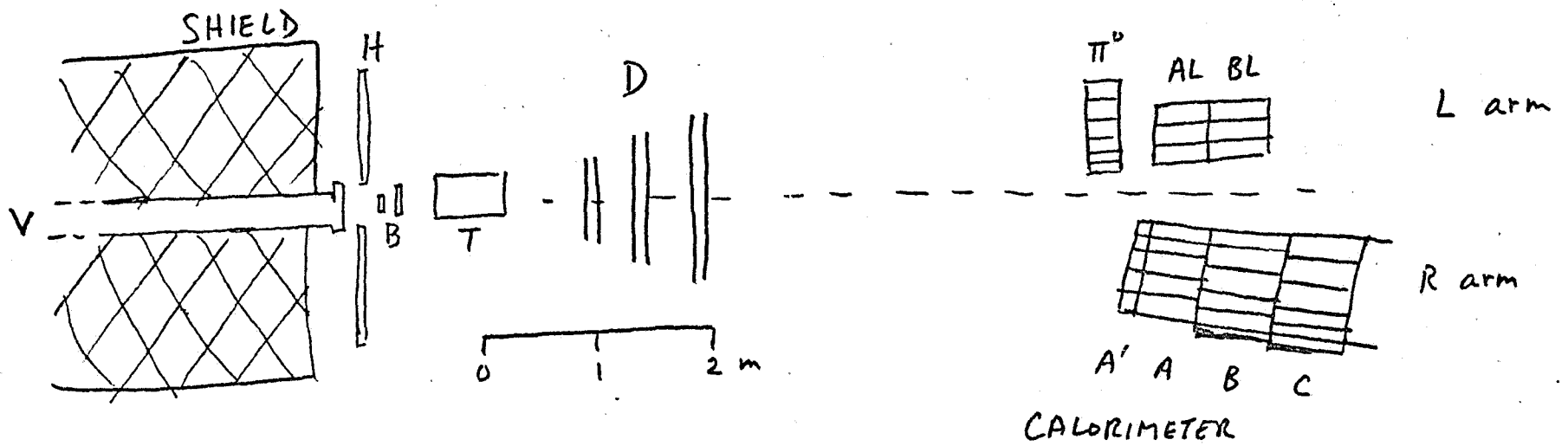


Fig. 1

SCHEMATIC PLAN VIEW OF APPARATUS (E-395).

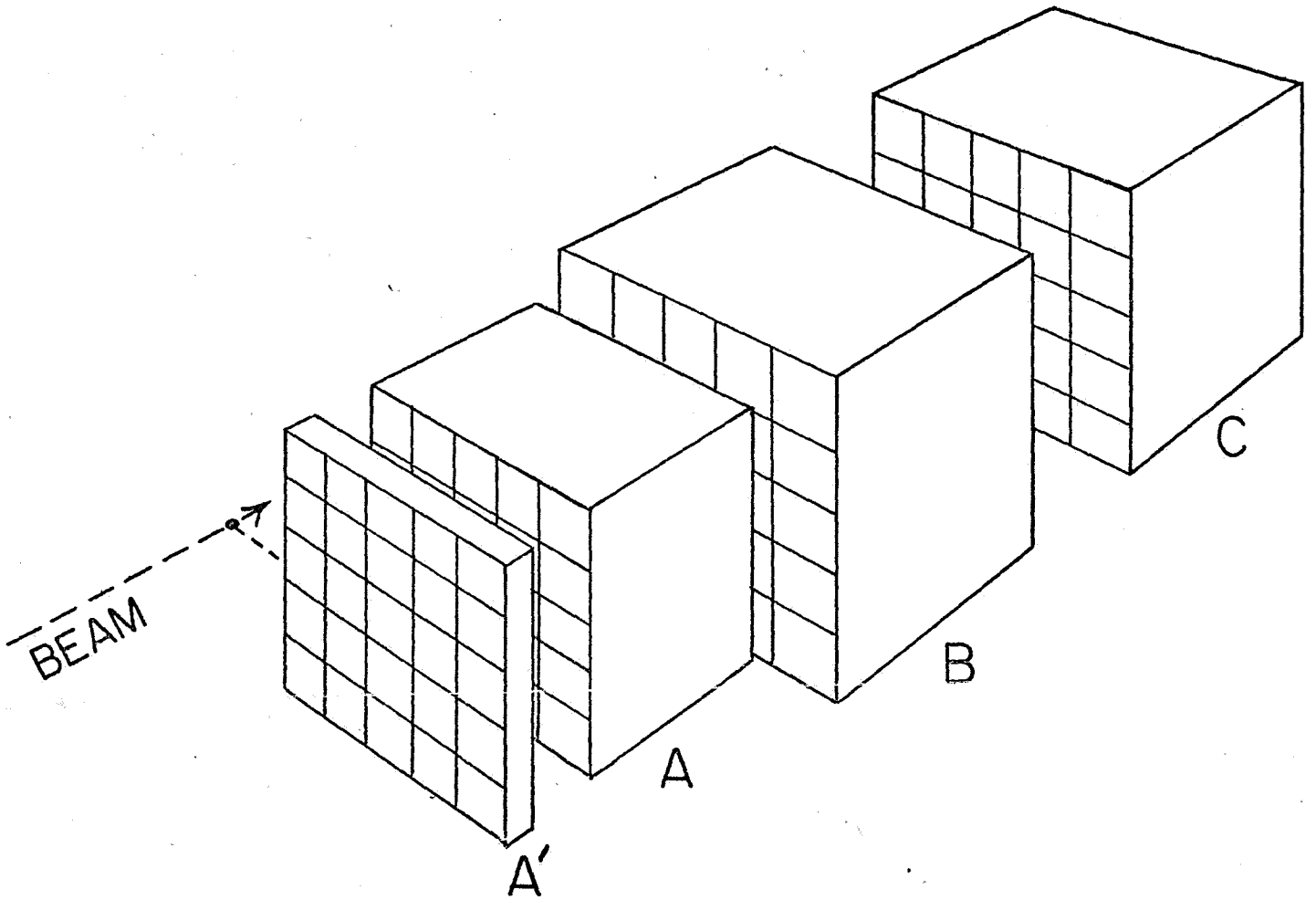


FIGURE 2. SCHEMATIC VIEW OF WEST HADRON CALORIMETER.

report<sup>(13)</sup>. In the present detector, the scintillator is "Plexipop"<sup>(14)</sup> and the fluorescent bars are made of "BBO"<sup>(15)</sup>-doped acrylic<sup>(16)</sup>. The photomultipliers are made to our design<sup>(17)</sup>, and are specially designed to allow them to be embedded in the calorimeter array without giving large spurious signals from particles hitting the photomultiplier.

The size of the individual modules, as well as the sampling frequency within the modules, was chosen by us after a series of extensive tests on energy resolution, shower size, and uniformity<sup>of</sup> response.<sup>(13,18,19)</sup> Each module gives response typically uniform to  $\pm$  a few percent over its entire volume.

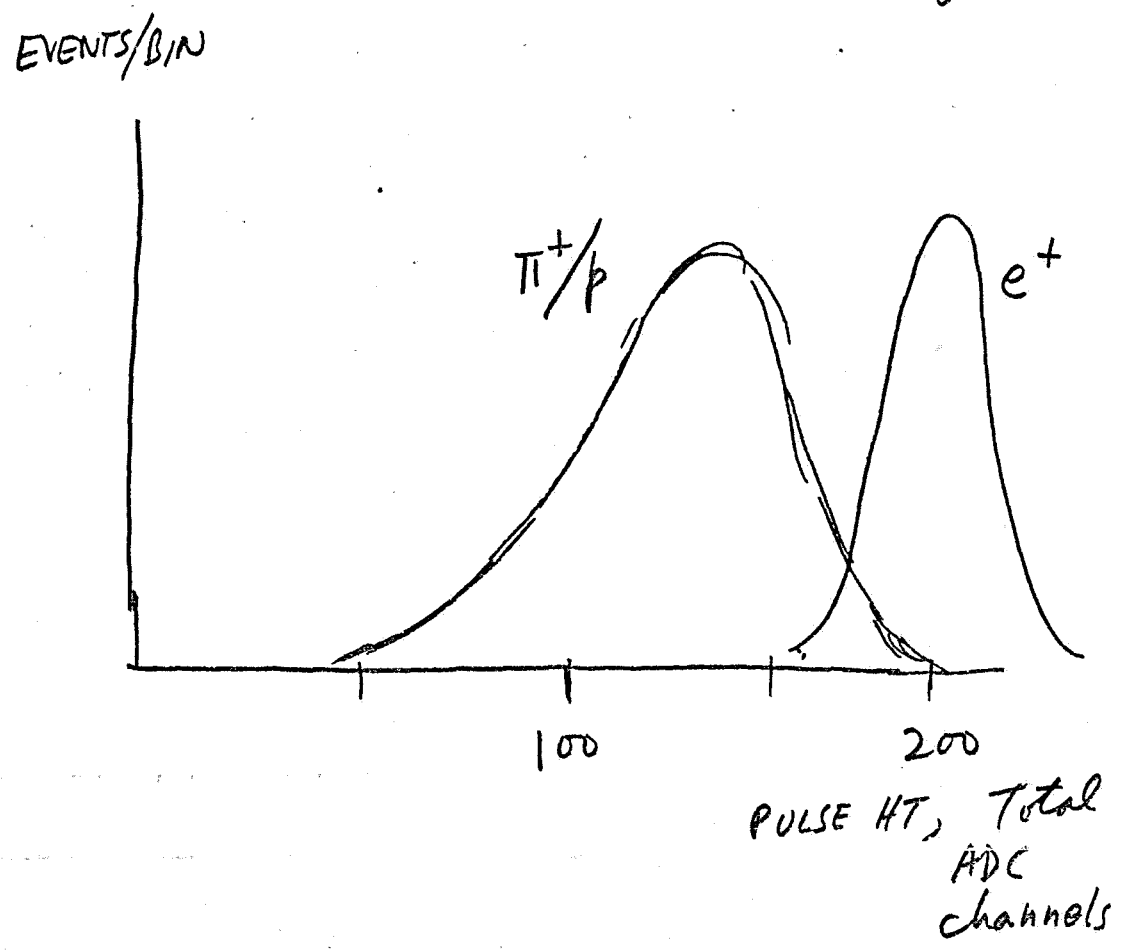
The detailed design of the calorimeter modules will be described by us elsewhere.

The basic method of energy calibration for the calorimeter uses both the pulse height response for minimum ionizing particles, and direct energy calibration using monoenergetic particle beams. The energy resolution has been measured, with monoenergetic beams, for a number of different entrance points into the array. For a typical particle energy of interest in the 400 GeV data, 20 GeV, the resolution corresponds to a  $\sigma$  which is about 6% for e-m showers and about 20% for non-e-m showers. This response is illustrated in Figure 3. It is to be stressed that for calorimeter use on events with a steeply falling  $p_T$  spectrum, an extremely important feature of the response is the absence of any extended "tail" on the pulse height spectrum. Any extended tail can make the resolution-unfolding problem so difficult as to be almost impossible. The present modules give effectively no tail whatsoever beyond the pulse height produced by purely e-m showers, and the resolution-unfolding problem is manageable without serious difficulty.

The LEFT (L) arm has 24 segments of electromagnetic shower detector calorimeter (a " $\pi^0$  detector"), followed, over a large part of its CM solid angle, by 4 absorption lengths of further calorimeter. The CM solid angle covered by the  $\pi^0$  detector is again about 1.5 sr; for hadrons the coverage is about 1 sr.

Between the hydrogen target (45 cm long for the data reported here) and the

Fig. 3



Pulse height spectra,  
20 GeV Single Particles. (R arm)

calorimeter, there were 6 planes of drift chambers. Four of these planes had "x" readout only (vertical wires); the other two had two-dimensional xy readout, using a delay-line readout system developed by M. Atac and associates<sup>(20)</sup>.

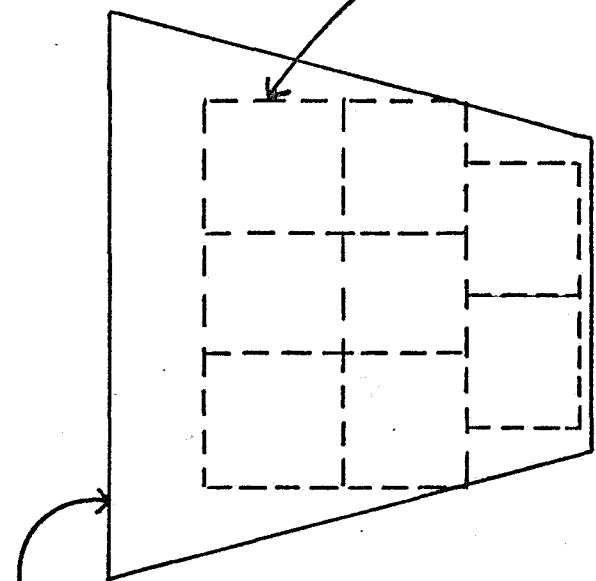
This array of chambers permits tracking charged particle trajectories to determine the vertex location. Presently this tracking, not yet refined, gives a vertex location typically accurate to a few cm or less, in z. Except for events with tightly clustered tracks, the drift chambers also give x, y coordinates for each charged track at the calorimeter. This tracking information is also not yet refined, but we find events sufficiently frequently with drift chamber tracks pointing directly at hadronic-type energy depositions in the calorimeter array so as to enable us to identify the character and rate of multi-particle high  $p_T$  events with very little uncertainty.

Finally, we show in Figure 4 a front view (beam's-eye view) of the two arms, and the solid angle coverage of the Right arm, in the "7 m" position. For the Right arm, the total solid angle covered, to the edges of the calorimeter array, is about 2 sr; a fiducial region, which omits the edge regions, is about 1.5 sr effective; the CM angular coverage per segment averages about 0.3 rad x 0.3 rad.

The drift chambers covered a considerably larger solid angle in each arm. At 400 GeV, the drift chambers covered over 4 sr, in each arm.

The character of the events we see at high  $p_T$  is described below, in section 5.

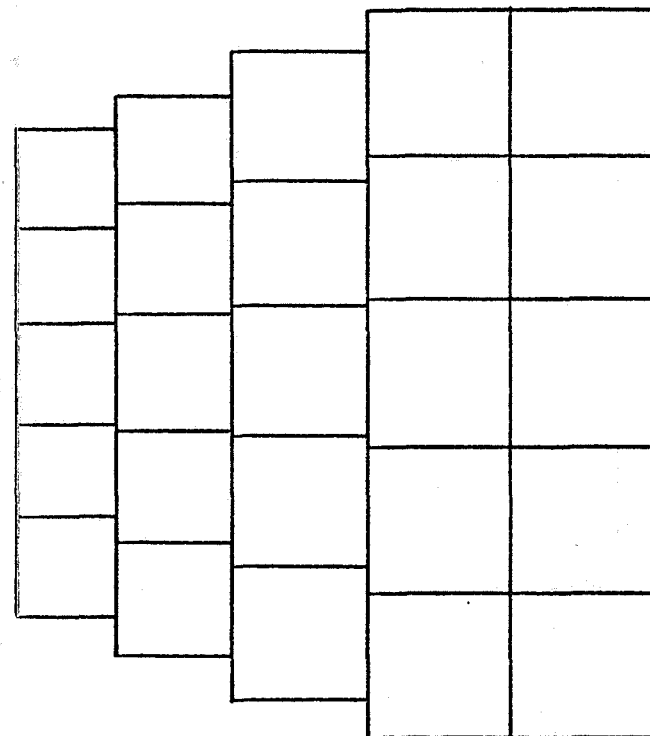
LEFT HADRON CALORIMETER



$\pi^{\circ}$  CALORIMETER:  
SUBDIVIDED 6 COLUMNS  
x 4 ROWS

$\oplus$   
BEAM

RIGHT HADRON CALORIMETER



1 meter

FIGURE 4-a. Calorimeter as seen from target, at 7.5 meters.

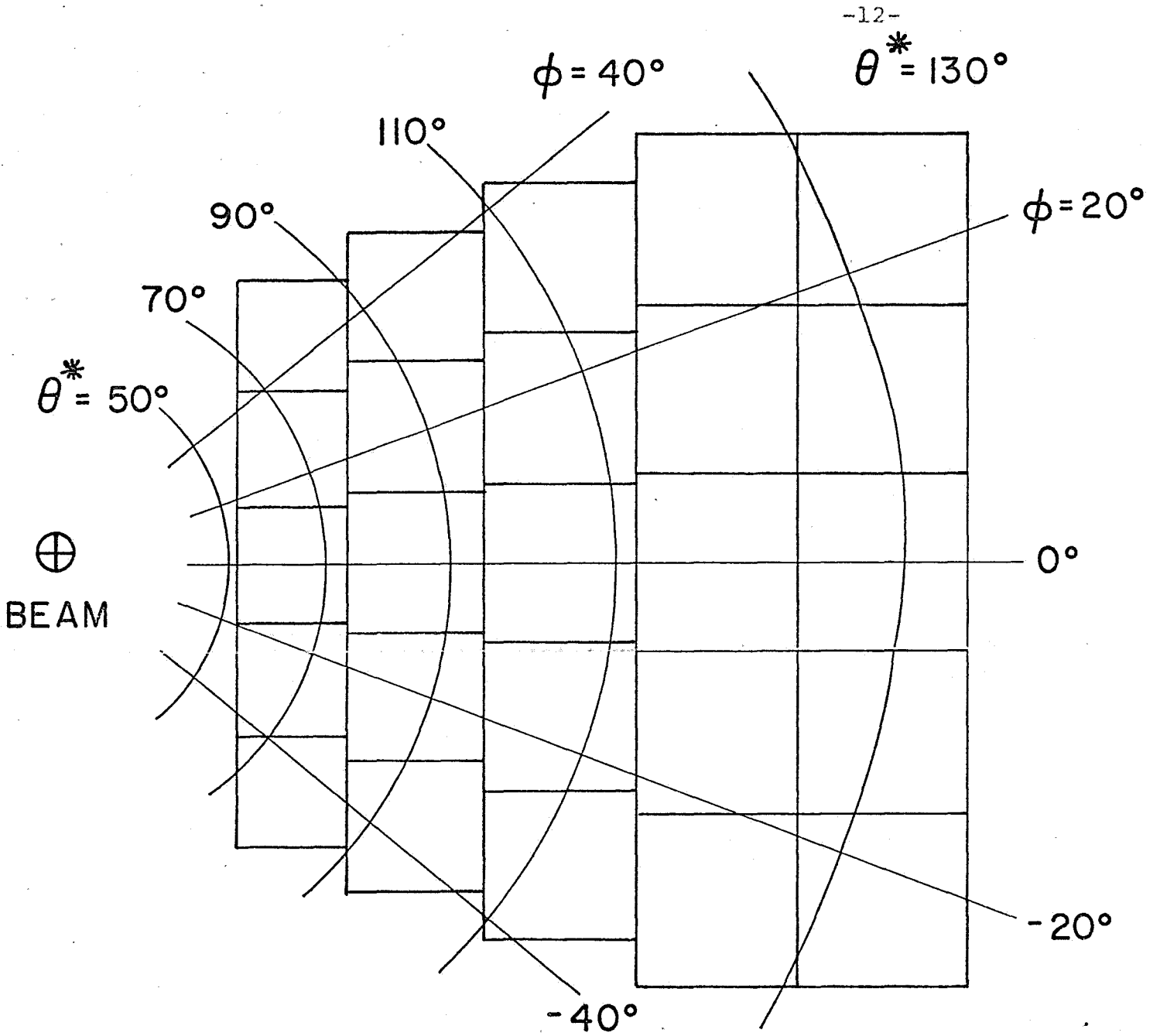


FIGURE 4-b. Front view of right calorimeter arm, showing center-of-mass angle coverage at 400 GeV (7 meter position).

### 3. TRIGGERING ARRANGEMENTS

Several types of triggers were used simultaneously. Triggers were made, and data recorded, in the following way. First, each photomultiplier signal was amplified, at the calorimeter, with a highly stabilized amplifier, of remotely switchable gain, and sent on to the counting room via very noise-free "Twinax" cables. The amplifiers permitted appropriate gain levels both for data-taking and for module calibration using muons<sup>(21)</sup>. The signal arriving in the counting room was then split, using passive fanouts, and used in two separate ways. One line, for each module, went to an ADC, which was gated on when a trigger occurred. The second line, for each module, was used to produce high  $p_T$  triggers of a variety of types. For example, a fast signal with amplitude corresponding to the total  $p_T$  reaching the Right arm was generated by first attenuating the signal from each module by an appropriate factor to give an output proportional to  $p \sin \theta_{LAB}$  for that module, then adding these weighted signals from all modules in that arm. The resulting "total-Right-arm- $p_T$ " signal did not depend on multiplicity in any way. Henceforth we shall designate such total- $p_T$  values by using a capital P--for example as  $P_T$ , or PTR (for  $P_T(\text{RIGHT})$ ).

Interactions were recorded for analysis if they met any one of four types of trigger requirements. All triggers required a coincident beam telescope signal and the appropriate signal above a  $P_T$  threshold. The types of triggers recorded were

- (1) L trigger: left arm only, large solid angle ( $\sim 1.5$  sr)
- (2) R trigger: right arm only, large solid angle ( $\sim 1.5$  sr)
- (3) "L+R" trigger: sum of magnitudes of left and right arm total- $p_T$  values, and
- (4) "SP" trigger--a "single-particle" trigger: left arm, small solid angle ( $\sim 0.1$  sr).

In normal data-taking, each of the first 3 of these 4 types of trigger simultaneously supplied signals to discriminators operating at three different threshold levels. Thus 10 different trigger channels were simultaneously open. (The triggers operating at lower thresholds were of course fed to the triggering input through pre-scalers, to provide modest triggering rates for these lower threshold channels.) The  $P_T$  levels used were, typically, about 1.5, 2.2, and 3.0 GeV/c for L triggers and for R triggers

We typically operated with a total beam rate of about  $0.7$  to  $0.9 \times 10^6$  particles per 1.2 second spill. Events were vetoed if a pileup gate fired, or if any of an array of halo counters fired, or if the  $dE/dx$  in the final beam telescope counter indicated that an interaction had occurred in the beam telescope counters. Under these conditions, and with the  $P_T$  thresholds set as indicated above, we typically recorded about 50 events per spill.

#### 4. BACKGROUND

For 400 GeV, 7 m position, the raw ratio (target-full)/(target-empty), dead-time corrected, was typically over 5:1, with the triggering mix described above. At the highest  $P_T$  values reached, somewhat above 5 GeV, the full/empty ratio was about  $2\frac{1}{2}$ :1 after two very simple software cuts, and before using any vertex requirement on the drift chamber tracks. These two cuts were the following:

- (1) The number of total "hits" in the drift chambers was required to be at least 14, corresponding roughly to the level occurring for 2-track events. (The delay line chambers give 2 "hits" for each track.)
- (2) Events were rejected, in software, if any one module recorded a signal greater than about 100 GeV energy deposition. (Such signals typically occurred from cosmic ray events, for example.)

We remark that background identification is greatly facilitated by the fact that the calorimeter array is segmented in depth as well as in area. That depth segmenting plays an essential role in allowing us to get almost no spurious events even at the 5 GeV/c  $P_T$  level, where events occur at about 10/hour, or about 1 in  $10^6$  interactions. The background rate is consistent with

an estimate for the rate expected from events produced in the final beam telescope scintillators, but which avoid the  $dE/dx$  veto. Those scintillators are 7% farther from the calorimeter than is the hydrogen target, and tracks reaching a particular calorimeter segment will correspondingly have a lower true  $P_T$  if they actually come from the scintillator rather than from the target. The result is a very slight effective shift in the true  $P_T$  being measured; the amount of the shift is small compared even to the modest uncertainty in our energy scale resulting from calorimeter resolution effects.

Examination of events left after the above two cuts shows that the great majority of them are multiple particle events, even at well above 5 GeV/c (R trigger), with no evidence of any spurious large signal from cosmic rays or other sources.

#### 5. CHARACTER OF SINGLE PARTICLE AND MULTI PARTICLE EVENTS AS SEEN IN THE CALORIMETER

As part of our calibration procedure, we have put beams of 10, 20 and 50 GeV particles into the Right arm, at several different positions.

A single particle entering the calorimeter gives in general a well localized shower as seen in a front view projection of the modules. We will show below examples of the distribution around the entering axis. Moreover, the segmenting in depth permits very clean separation between  $\pi^0$ 's and non- $\pi^0$ 's--the gamma rays from a  $\pi^0$  deposit their energy completely in the A' and A layers, typically with a substantial fraction of the energy in the A' layer. Non- $\pi^0$ 's, on the other hand, give showers which typically penetrate much more deeply, and which give very little energy in the A' layer.

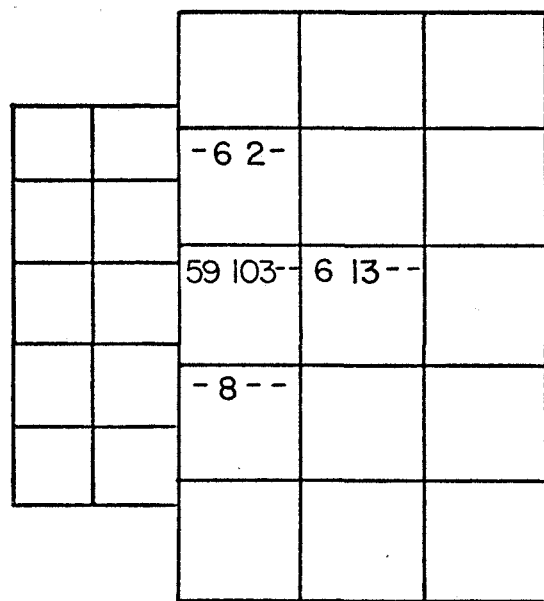
Multi-particle groups entering the calorimeter thus typically show quite clearly separated showers for individual particles, for multiplicities up to 3 or 4. At higher multiplicities one begins to get appreciable overlap of the individual particle showers. We have spoken so far only of the calorimeter alone;

of course the drift chamber tracks assist greatly in identifying the multiplicity involved, and in enabling us to identify the  $P_T$  values of the individual entering particles, and the relative momenta of those particles with respect to each other.

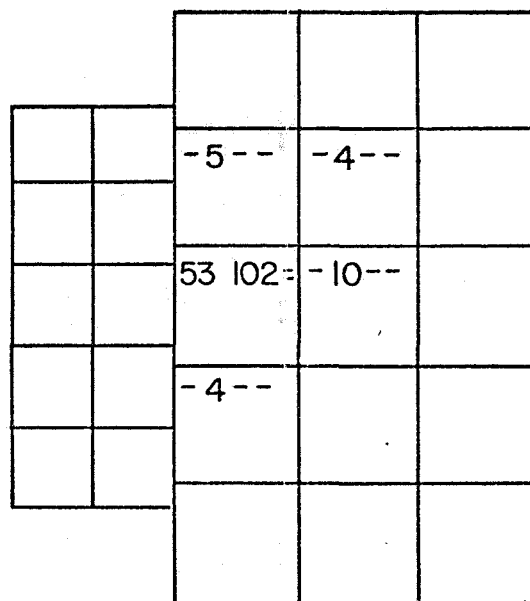
The character of the energy deposition for individual  $e^+$  and individual  $\pi^+$  or protons is shown for typical events in Figure 5. These events were taken with a monoenergetic 20 GeV beam of mixed  $\pi^+/p$  and  $e^+$  entering the calorimeter, in the center segment of column 3, but over toward the neighboring segment in column 4. The direction of the particle beam for these events was not face on into the calorimeter, but angling somewhat toward the right. The units shown are roughly in GeV deposited in the individual modules. We have used a conversion factor of 10 ADC channels per GeV for electromagnetic deposition, and 8 channels per GeV for nonelectromagnetic deposition. (These numbers closely approximate the correct energy scale as determined by our overall calibration measurements. The numbers used for determination of the energy of an event or a spectrum are also adjusted to take into account the folding effect of the calorimeter resolution into the  $P_T$  spectrum.) From the examples shown in Figure 5 one can understand qualitatively how single-particle showers can be identified in the calorimeter, and how well the energy can be determined. Note that slightly different energy scales per ADC channel must be used for e-m and non-e-m showers, to give the best estimate of particle energy.

In Figure 6 we show a few examples of multi-particle events triggering the R arm, as recorded under actual data taking conditions. These events are chosen as representative of events with  $P_T$  (R) in the vicinity of 5 GeV/c.  $P_T$  here designates the magnitude of the vector sum of the individual  $P_T$ 's shown by the modules of the R arm.

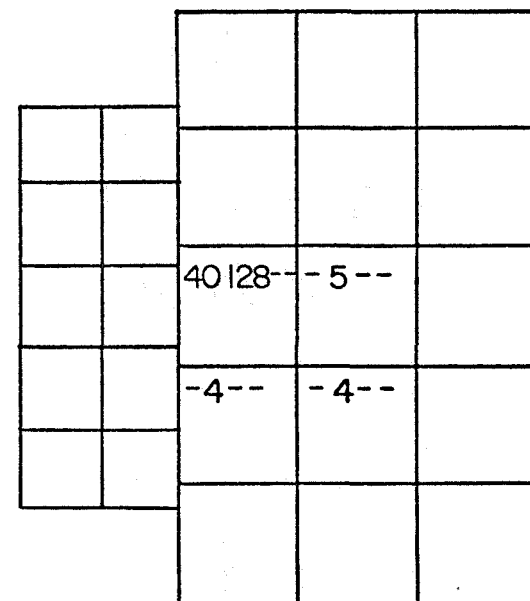
Figure 6a is actually an example, among events with  $P_T = 5$  GeV/c or so, of a case with the individual particle showers somewhat better separated than is typical for this value of  $P_T$ . This event shows several features commonly seen in these high  $P_T$  events. (1) Part of the energy is electromagnetic,



(a)



(b)

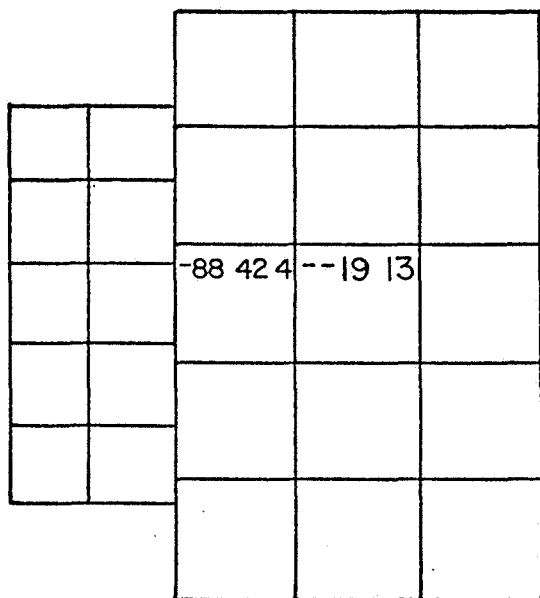


(c)

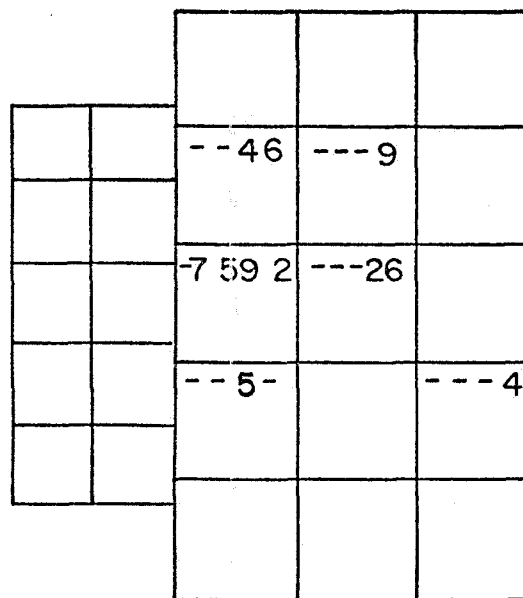
TYPICAL EVENTS, 20 GeV  $e^+$

NUMBERS SHOWN ARE ADC SIGNALS, IN CHANNELS.  
 FORMAT: A' ABC

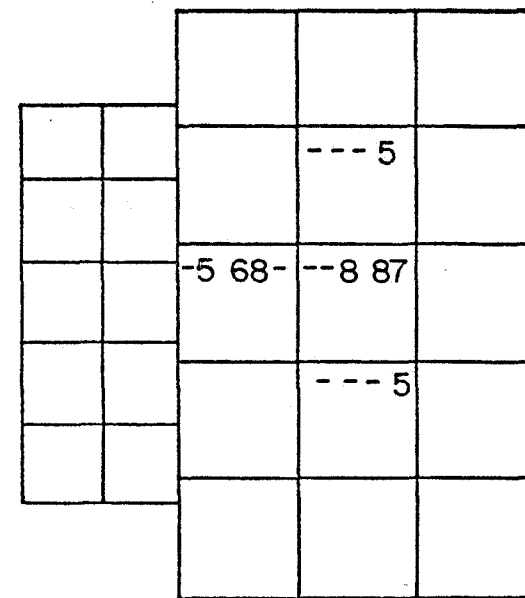
FIGURE 5-a,b,c



(d)



(e)



(f)

TYPICAL EVENTS, 20 GeV  $\pi^+$  or p

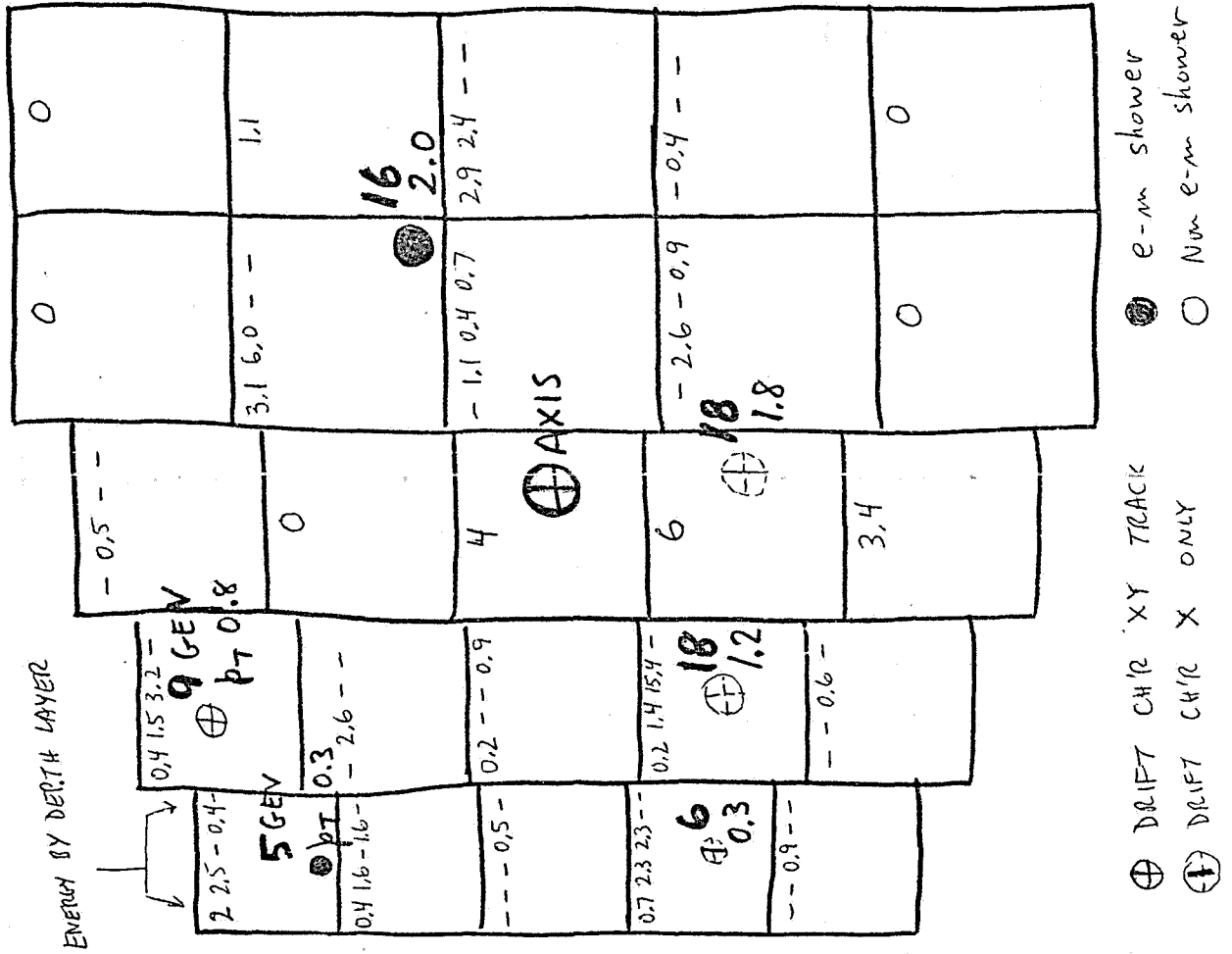
NUMBERS SHOWN ARE ADC SIGNALS, IN CHANNELS.

FORMAT: A'ABC

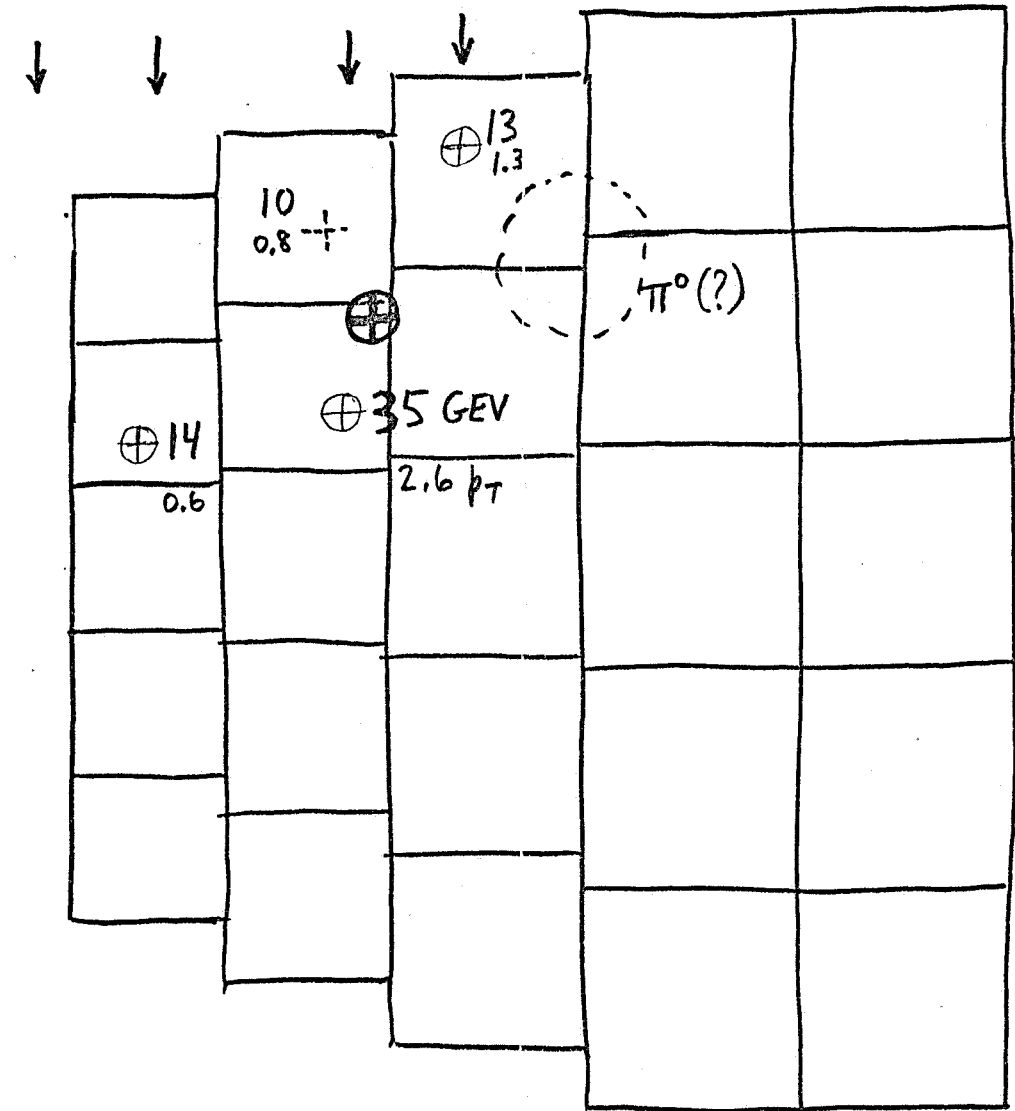
10603-835

FIG. 6a

72 GEV  
 $PTL = 5.3$   
 $(PTL = 2.3)$   
 $(\sum |p_T^{(i)}| = 6.4)$



TYPICAL 5 GeV/c EVENT  
 [A bit more spread out than typical]



72 GEV  
 PTR = 5.0  
 (PTL = 2.8)  
 4.7 GEV PT  
 IN  $\frac{1}{8}$  SR  
 (35 GEV, 13 GEV, 10 GEV)

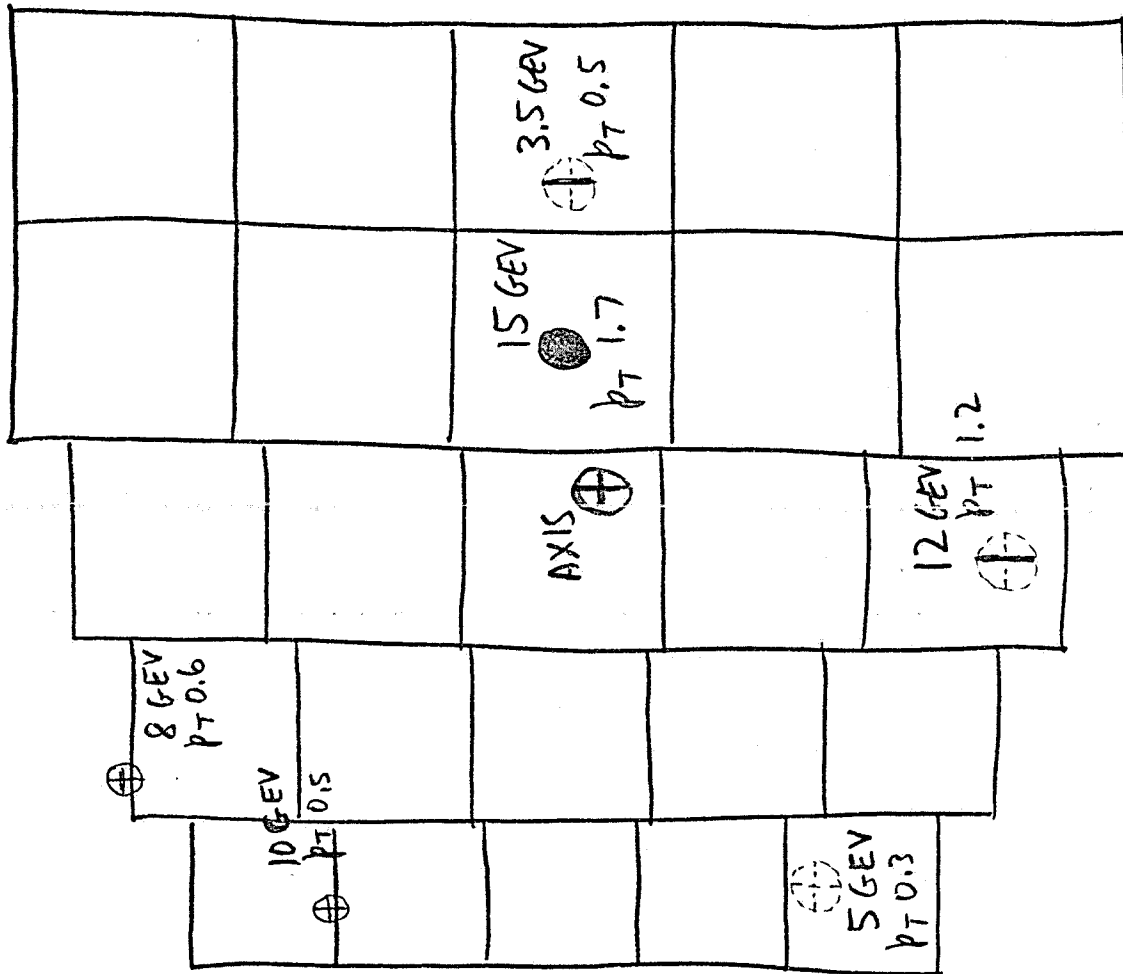
[Typical 5 GeV/c event]  
 [More compact than typical -- and cleaner tracks]

Fig. 6b

FIG. 6c

10603-967

54 GEV  
PTR = 4.1  
(PTL = 2.3)



TYPICAL 4 GEV/c EVENT

(FOR LEGEND SEE FIG. 6a)

$\sim 2.0$  GeV  $p_T$  in this case, and is visible as 2 separate  $\gamma$  showers. The separation of these showers is consistent with their being the two  $\gamma$  rays of a  $\pi^0$ . (2) Several distinct non-e-m energy depositions are visible. One of these, spreading over some 4 segments, could correspond to one hadronic shower or perhaps to more than one; the drift chambers show clear evidence of one or more tracks aiming at the calorimeter at the x position of the "center of gravity" of that cluster. The y coordinate for this "track" did not correspond to the calorimeter cluster--that can happen if more than one track hits a single wire of an xy plane. The total  $P_T$  of this cluster is approximately 1.8 GeV/c. (3) There are 2 or 3 other rather distinct localized regions of energy deposition. Two of these would clearly occur on the same wires of the drift chamber set. The drift chamber tracks give one xy coordinate (one would be lost if two charged tracks hit the same wire cell) for this pair, and it aims directly at the location of the calorimeter energy deposition for one of the localized groups. (4) In summary, the event shows (a) a clear probable  $\pi^0$  of  $p_T = 2.0$ , (b) a probable hadron (i.e., non  $\pi^0$ ) of  $p_T = 1.8$  (or possibly two near-by hadrons totaling this  $p_T$ ), (c) two other hadrons of  $p_T = 1.2$  and  $0.8$ , and (d) two other localized groups of lower  $p_T$  each,  $0.3$  and  $0.3$ .

It is characteristic of the great majority of events in the upper end of the  $P_T$  range we cover, i.e., in the vicinity of 5 GeV/c  $P_T$ , that each event shows a multiplicity, and a distribution of individual particle  $p_T$  values, similar to those of the events in Figure 6. That is, for  $P_T$  around 5 GeV/c, one finds typically a total multiplicity of 5 or 6 in the calorimeter, evidence for 2 or 3 particles each with  $p_T$  above 1 GeV/c, and 2 particles or so with "low"  $p_T$  values, 0.3 GeV/c or so.

A further characteristic of great interest concerns the question of how closely the individual particles for each event cluster near each other, in direction. To examine this question, we have defined a "cluster axis" for each event, and examined the distribution of individual  $p_T$  vectors with respect to that axis. In the next section we discuss this question in more detail.

6. THE "JET AXIS", AND THE DISTRIBUTION OF PARTICLE ANGLE  $\alpha$  FROM THE AXIS.  
INTERNAL INDIVIDUAL-PARTICLE TRANSVERSE MOMENTA.

We have calculated the direction of the total vector momentum entering the calorimeter in each event. For brevity, and at the moment with no prejudice as to what a "jet" is, we shall call this direction the "jet axis". To explain specifically: we calculate the average rapidity (effectively the average polar angle), and the average azimuthal angle  $\phi$  of the cluster. These averages are calculated by weighting the rapidity and  $\phi$  of each individual module by the amount of  $p_T$  deposited in that module.

A central question, which we now begin to examine here, is the detailed manner in which the individual particle  $p_T$ 's do or do not cluster closely to the jet axis. Putting aside for the moment the question whether a better procedure could be used to choose an optimum direction for the jet axis, we proceed to describe the results with the definition given above.

With the jet axis defined as above, namely the direction of the average rapidity and average azimuth of all particles reaching the calorimeter, we define an angle  $\alpha$ , between the jet axis and each individual modular deposition. We then calculate the  $\cos \alpha$  distribution for a group of events. In Figure 7A we show this experimental distribution both for our normal trigger events (curve b) and for truly single-particle events--events using a calibration beam directed into the calorimeter (curve a). Both these curves are normalized to area = 1.0. In Figure 7B we show curves for data events chosen from three different  $P_T$  bands. In each of the curves in Figure 7B the curve is normalized to total area =  $P_T$ .

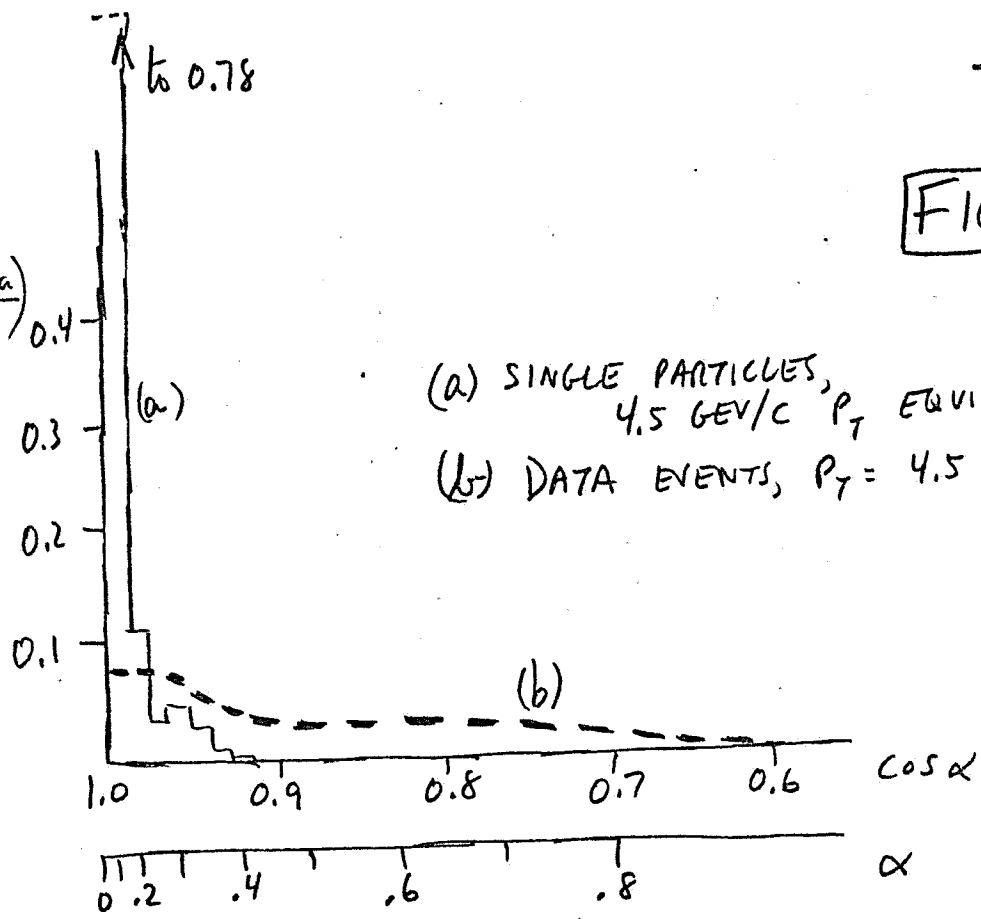
It is clear that the  $\cos \alpha$  distribution for the typical 5 GeV/c data event we observe is strikingly different from that for single-particle events. The single-particle events show a very sharply localized  $\cos \alpha$  distribution--the central  $\delta$ -function-like bump has a width coming from the finite segment area and from the shower size (which is roughly the same as the module transverse dimension); there is a tail, of small fractional area, coming from the way in which some fragments of the cascade shower in the calorimeter spread out an appreciable distance from the entering particle's trajectory.

FIG. 7

$$\frac{1}{A} \frac{\Delta A}{\Delta \cos \alpha}$$

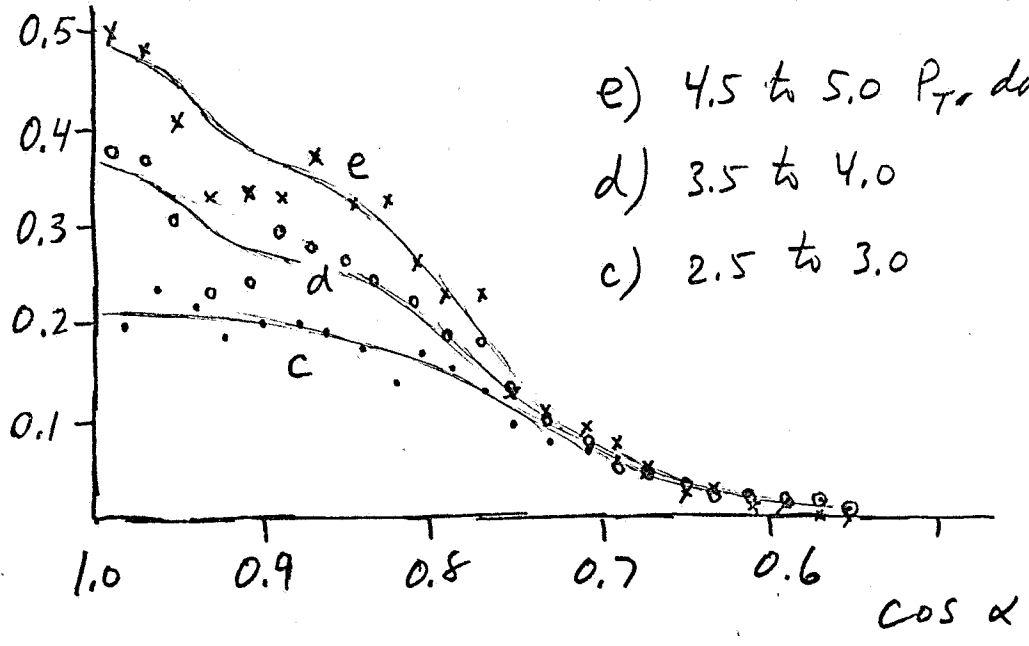
(fractional area)  
0.01

7A)



$$\frac{\Delta P_T}{\Delta \cos \alpha} \left( \frac{\text{GeV/c}}{0.02} \right)$$

7B)



PRELIMINARY RESULTS  
E-395

The data events, on the other hand, show a  $\cos \alpha$  distribution representative of a multi-particle group, with the highest 40-50% of the total  $P_T$  occurring in the interval  $\cos \alpha = 1.0$  to  $0.9$ , corresponding to  $\alpha < \sim 0.45$  radian.

We remark that various other procedures could be used to choose a jet axis. The typical events going into Figure 7 show a central "core", with most of the total  $P_T$  in it, and 2 or 3 "outlying" low- $p_T$  particles, about  $0.3$  GeV/c each. These outlying particles typically pull the jet axis some appreciable amount away from the more concentrated core. Examination of a few typical events shows that if one locates an alternate jet axis more nearly centered in the core, then this axis is typically some 10 degrees or so from the one originally defined, and the result is to generally sharpen up the  $\cos \alpha$  distribution relative to that of Figure 7. E.g., moving the jet axis 10 degrees CM ( $0.2$  radian) typically results in changing some individual  $\alpha$  values for higher- $p_T$  particles downward, from an initial  $0.4$  to  $0.6$  radians down to the  $0.25$  to  $0.45$  range. This change (a) concentrates the  $\cos \alpha$  distribution in the range below  $(1 - \cos \alpha) = 0.1$  rather than  $0.2$ , and (b) gives the individual high- $p_T$  particles much smaller values of "internal transverse-momentum" relative to the jet axis.

It is clear from these studies done so far that (1) the exact shape of the distribution depends sensitively on the exact method of defining a jet axis, (2) nevertheless, typical  $5$  GeV/c  $P_T$  data events have a multiparticle character, totally different from that for single particle showers of similar  $P_T$ , (3) in the typical  $5$  GeV/c data event, some 70% of the total  $P_T$  lies in a central core, of typically 2 or 3 particles, within the range  $\alpha_{\text{effective}}^{\text{(core)}} \sim 0.3$  to  $0.4$  rad, corresponding to a solid angle of the order of  $1/3$  to  $1/2$  sr.

Finally, we remark on the numerical value of the internal transverse momentum for individual particles with respect to the jet axis. As we have just said, in the typical event around  $P_T = 5$  GeV/c, there is a "core", with 2 or 3 particles lying in a solid angle of about  $1/2$  sr, with these particles making individual angles  $\alpha$  less than  $0.3$  to  $0.4$  rad from the jet axis. In the typical 3-particle core case the individual core particles have  $p_T$  values between about  $1.0$  and  $2.0$  GeV/c; and they have individual transverse momenta from the axis averaging typically  $0.3$  or  $0.4$  GeV/c.

7. RELATIVE RATES OF MULTIPLE-PARTICLE AND SINGLE-PARTICLE HIGH  $P_T$  EVENTS.

We have found, in agreement with reference 7, that the great majority of our high  $P_T$  events, when we use an entire arm of the calorimeter as a trigger, have multiple particles entering the calorimeter. In order to observe the relative cross section for single particles, we used also a trigger which responded only to the  $P_T$  deposited in a small section of the left arm, a "Single Particle" (SP) trigger. This SP trigger corresponded to an effective solid angle of about 0.1 sr (CM) for  $\pi^0$ 's, and somewhat less for hadrons.

Using the SP trigger, we measured the cross section for  $\pi^0$ 's, over a certain  $p_T$  range. The results, and a comparison with some other reported measurements<sup>(22,23)</sup>, are shown in Figure 7A. We observe good agreement, within a factor of about 2, which corresponds to a systematic uncertainty of 5 to 10% in the energy scale for the preliminary analysis reported here.

For single  $\pi^0$ 's, at about  $90^\circ$  CM, we thus measure an invariant  $\sigma$ ,  $\sigma_I$ , of about  $3 \times 10^{-30} \text{ cm}^2/(\text{GeV})^2 \cdot \text{sr}$  at 2 GeV  $p_T$ , and a value of

$$\frac{\Delta\sigma}{\Delta p_T} \approx 6 \times 10^{-31} \frac{\text{cm}^2}{\text{GeV}} , \quad \left\{ \begin{array}{l} 0.1 \text{ sr} \\ \text{single } \pi^0 \\ 2 \text{ GeV } p_T \end{array} \right.$$

From the data of Antreasyan et. al.<sup>(24)</sup> we note that if we sum over all particle species this would correspond to

$$\frac{\Delta\sigma}{\Delta p_T} \approx 2.4 \times 10^{-30} \frac{\text{cm}^2}{\text{GeV}} , \quad \left\{ \begin{array}{l} 0.1 \text{ sr} \\ \text{sing. part. all species} \\ 2 \text{ GeV } p_T \end{array} \right.$$

We now compare this with the cross section we measure when we use the "L" trigger, the entire left arm. We then get

$$\frac{\Delta\sigma}{\Delta p_T} \approx 6 \times 10^{-28} \frac{\text{cm}^2}{\text{GeV}} , \quad \left\{ \begin{array}{l} \sim 1 \text{ sr} \\ \text{all high } P_T \text{ events} \\ 2 \text{ GeV } P_T \end{array} \right.$$

Thus when we increase the detector solid angle 10-fold, the (multiple-particle) cross section increases about 250-fold, compared to the all-species sum cross section at the smaller solid angle, at 2 GeV  $P_T$ .

We obtain results of similar nature with the Right arm, and also at higher  $P_T$ .

To interpret the multiple-particle cross section in terms of an invariant cross section requires a more careful examination of fiducial region solid angle acceptance. This is taken up in Section 9, below. At this point, however, we simply note again that in calorimeters of the relatively large solid angle we have, high- $P_T$  events are very heavily dominated by multiple-particle groups, with the experimental  $\Delta\sigma/\Delta P_T$  ( $\text{cm}^2/\text{GeV}$ ) for an entire arm being of the order of 100 times the single- $\pi^0$  cross section which a detector of that total solid angle would have.

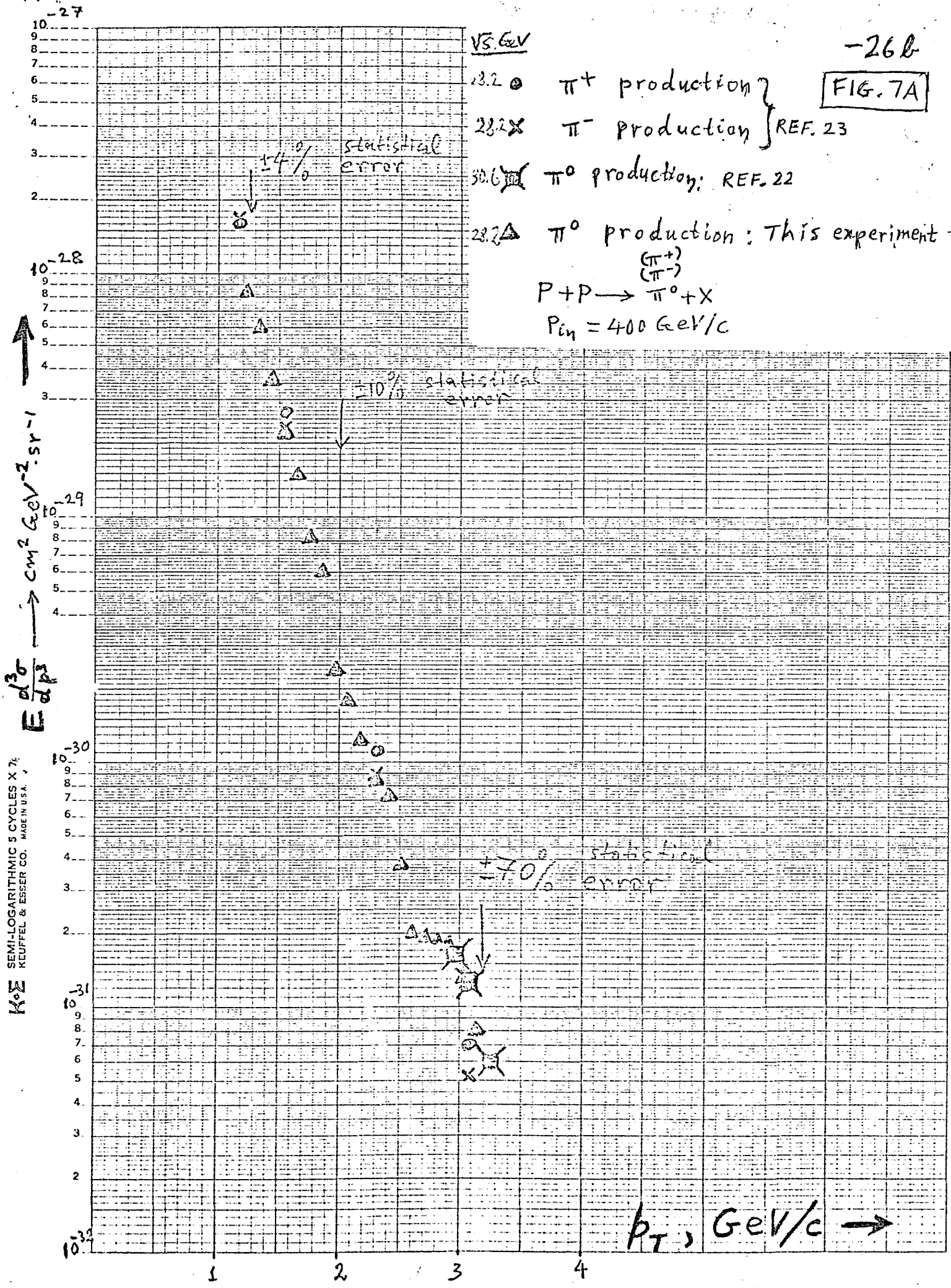
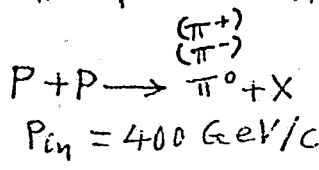
FIG. 7A

VS. GeV

- 23.2 ●  $\pi^+$  production
- 23.2 X  $\pi^-$  production
- 30.6  $\pi^0$  production: REF. 22
- 28.2  $\Delta$   $\pi^0$  production: This experiment

REF. 23

REF. 22



KEE SEMI-LOGARITHMIC 5 CYCLES X 7/8 KEUFFEL & ESSER CO. MADE IN U.S.A.

$\frac{d^3\sigma}{dp^3}$   
 $\text{cm}^2 \text{GeV}^{-2} \text{sr}^{-1}$

$p_T, \text{GeV}/c \rightarrow$

8. ARE THE EVENTS "JET"-LIKE IN THE FORM PREDICTED BY BJORKEN ET. AL.?

The predominant features of the high  $P_T$  groups we see are these:

- 1) A multiparticle group, carrying in total up to 40-50% of the initial beam energy ( $\frac{1}{2} \sqrt{s}$ ), comes out of the interaction going roughly sideways to the beam, and carries a large  $P_T$  into a small solid angle-- $3\frac{1}{2}$  to 4 GeV/c into about  $1/2$  sr.
- 2) Several particles in the group carry individual  $p_T$ 's which are unusually large (1 to 2 GeV/c); individual single particles with these high  $p_T$  values enter the detector (1.5 sr) in about 1% (1 GeV/c) to 0.1% (1.6 GeV/c) of all interactions.
- 3) The probability for several such high- $p_T$  particles to a) be produced, and b) enter the same small  $\Delta\Omega$  as each other, and c) be accompanied typically, in the same 1 sr region, by 2 to 3 additional particles totaling 1 to  $1\frac{1}{2}$  GeV/c, is experimentally  $\sim 10^4$  times larger than it would be if these particles were totally uncorrelated. That is: we are observing highly correlated groups of high- $p_T$  particles.
- 4) The calorimeter shows that outside of the main  $1/2$  sr core region, with 5 or so particles in it at  $P_T \sim 5$  GeV/c, there are typically one or two additional low  $p_T$  particles in the remaining 1 sr or so of the calorimeter, and 1 or 2 additional charged particles in the additional 2 sr covered by the drift chambers. With this evidence as to a concentration of track multiplicity, and with close to half the initial  $E^*$  ( $=\frac{1}{2}\sqrt{s}$ ) concentrated in  $\frac{1}{2}$  sr or so, it is clear that the clusters of particles we see represent single isolated multiparticle groups, with  $\Delta P_T/\Delta\Omega$  of the order of 5 GeV/0.5 sr. For these events there can clearly be no other multiparticle groups, in the trigger-side hemisphere, with correspondingly intense  $\Delta P_T/\Delta\Omega$ .
- 5) The  $\cos \alpha$  distribution for events of total  $P_T$  ranging from 2.5 to 5 GeV/c shows that in the central  $1/2$  sr the value of  $\Delta P_T/\Delta\Omega$  increases with the total  $P_T$  of the event.

6) We can define an axis for the group, as discussed above. In the typical 3 to 5 GeV  $P_T$  event, each of the particles in the central  $1/2$  sr or so carries a transverse momentum away from this "jet axis", i.e.,  $p_i^* \sin \alpha$ , which is of average magnitude about 0.4 GeV/c.

The above features correspond closely to what has been predicted by Bjorken for jets arising from scattered partons. While with the present apparatus we cannot exclude the possible occurrence of other types of high- $P_T$  events which would not show these high values of  $\Delta P_T / \Delta \Omega$  in a localized region, we can conclude that those high  $P_T$  events which dominate our triggers do indeed have

- a) the concentrated  $\Delta P_T / \Delta \Omega$ , and
- b) an inner structure

which correspond quite well to the main characteristics of the "jet" events which were predicted by Bjorken.

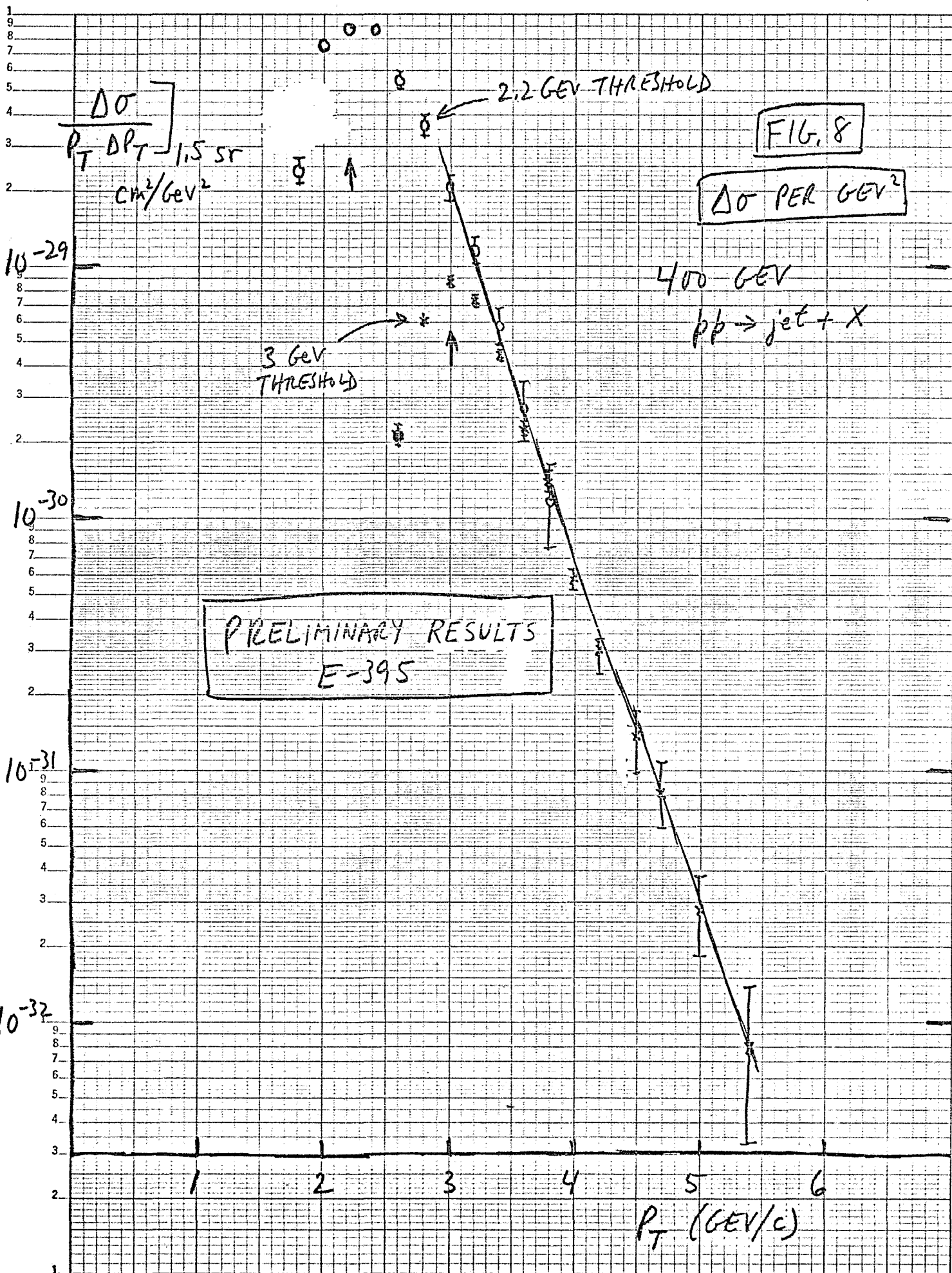
## 9. CROSS SECTION FOR JETS

We give here our preliminary cross section values for the data taken at 400 GeV, 7m position, with an R trigger. See Figure 4b for the angular coverage of the detector.

From the measured target-full rates we have subtracted a background, by comparing target-full and target-empty  $P_T$  spectra per unit "live beam flux". For the R trigger, this background is about 20% of the total event rate up to  $P_T = 3$  GeV/c, and then increases to a constant 40% above 4 GeV/c.

We then calculate a differential cross section for the 1.5 sr right arm, in the form  $\left[ \Delta\sigma_{jet} (GeV)^2 \right]_{1.5sr} = \frac{\Delta\sigma}{P_T \Delta P_T} \Big|_{1.5sr}$ . Note that this quantity is not an invariant cross section, but is an experimental quantity which can be compared with data measured by any other experiment which uses a calorimeter detector with the same solid angle coverage. The resulting values are plotted in Figure 8.

We also give a rough set of values for the invariant cross section,  $\sigma_I$ . To estimate this quantity we must know the effective solid angle  $\Delta\Omega$  for "containing" jets. From detailed study of the density of events in a plot showing the location of the jet axis in  $\theta^* - \phi$  space, we find a central region,  $20^\circ \times 20^\circ$  in size (the right arm has a total coverage roughly  $80^\circ \times 80^\circ$ ), in which the density of events is approximately uniform, and much higher than the density over the much larger region outside the this central region. (See Figure 9.) One might thus be led to use this 0.1 sr or so as a fiducial region. This region typically contains about 1/3 of all the events in a given  $P_T$  band, although it is only about 1/15 of the total solid angle of the right arm. We will give a rough estimate of  $\sigma_I$  based on this approach. But we emphasize that even the existence of a substantial plateau-like region of this kind by no means guarantees that jets of any given  $P_T$  are being "contained". It is of course impossible even in principle to either fully contain a large-angle jet, or to know accurately what particles entering the calorimeter may be coming from "beam jets" rather than from the main jet being detected. The question as to what is the "true  $\sigma_I$ " for jet production



46 6210  
 KEUFFEL & ESSER CO.  
 KEUFFEL & ESSER CO.  
 KEUFFEL & ESSER CO.



involves this fundamental uncertainty. We remark that there is another uncertainty, of similar magnitude, which has to do with the definition of the "energy" of the jet--that uncertainty arises because the sum of the center-of-mass energies of the individual fragments of a jet is larger than the magnitude of the vector sum of the momenta of those fragments. This effect by itself can introduce typically a 10 to 15% difference between  $|\vec{P}_T|$  and what one could call the "energy" of the jet,  $\sum p_i^*$  (neglecting rest masses of the fragments).

For these reasons, a sharply defined quantity like our  $[\Delta\sigma \text{ per } (\text{GeV}^2)]_{1.5 \text{ sr}}$  and similar quantities, will probably prove of greater use in describing jets and comparing results from different experiments, in the immediate future, rather than a value for the presumed  $\sigma_I$ . Nevertheless, we give here the value of  $\sigma_I$  which would result from our data if we use the central plateau-like 0.1 sr, and if we use the  $\Delta\sigma$  corresponding to events with the jet axis lying in that solid angle. We thus define a  $\sigma_I$  by

$$\sigma_I(\text{apparent}) = \frac{\Delta\sigma_{\text{jet axis in central } 0.1 \text{ sr}}}{P_T \cdot \Delta P_T \cdot \underbrace{\Delta\Omega_{\text{central}}}_{= 0.1 \text{ sr}}}$$

$\Delta\sigma$  in this central region is, as we have said, about 1/3 of  $[\Delta\sigma]_{1.5 \text{ sr}}$ . (It is curious, and grounds for caution, that this 1/3 value does not appear to change significantly for  $P_T$  varying from 2.5 to 5 GeV/c.) We thus obtain the simple result that  $\sigma_I(\text{apparent})$  defined in this way is simply about  $\frac{1/3}{0.1}$ , or 10/3, times the "harder" number,  $(\Delta\sigma \text{ per } \text{GeV}^2)_{1.5 \text{ sr}} = \frac{(\Delta\sigma)_{1.5 \text{ sr}}}{P_T \cdot \Delta P_T}$ .

If in fact even this central 0.1 sr does not represent a region of 100% efficiency for containing the jets, then the true  $\sigma_I$  describing jet production will be larger than the  $\sigma_I(\text{apparent})$  we are calculating. We have reason to believe that this is in fact the case.

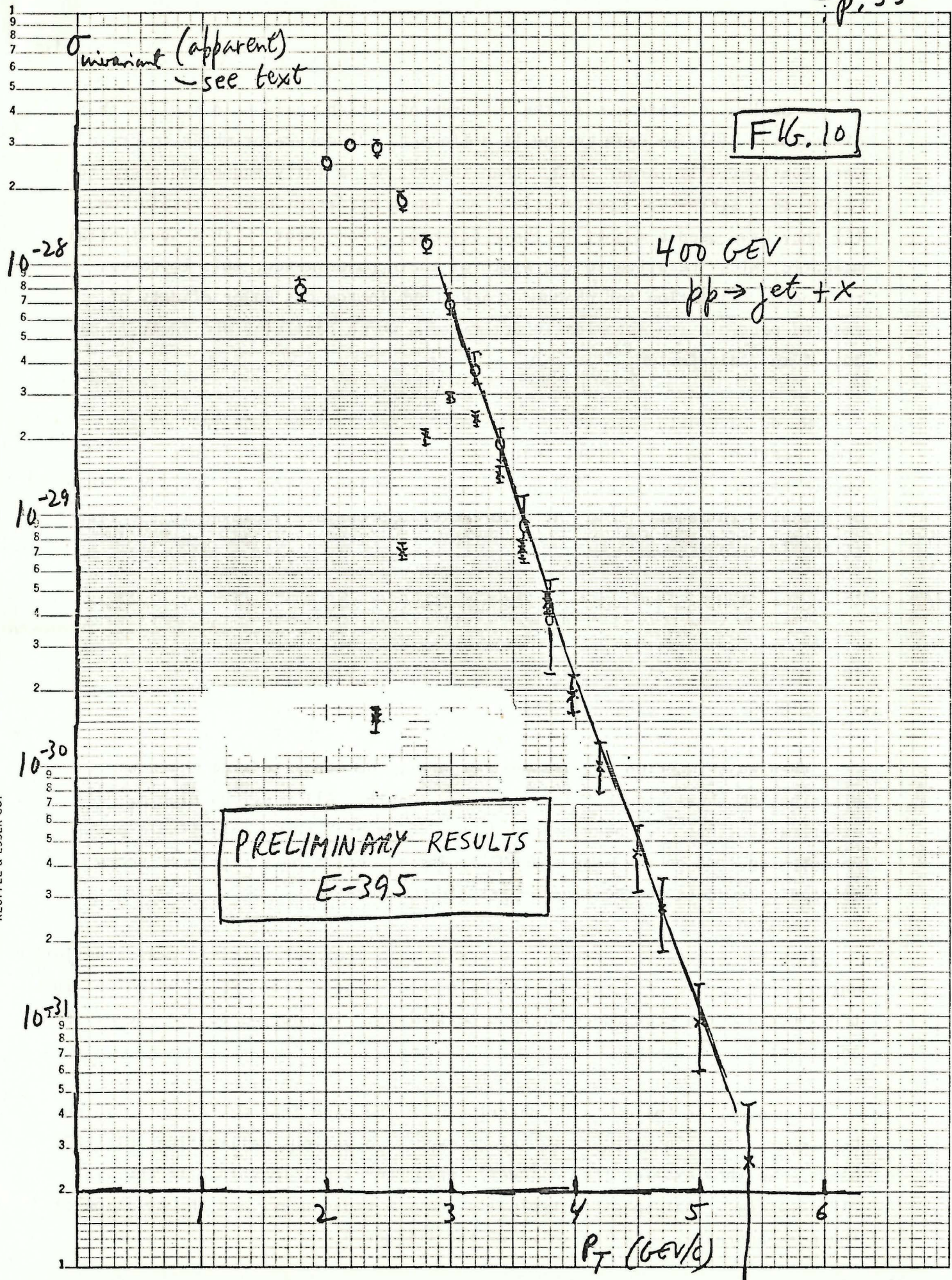
In any event, we plot  $\sigma_I(\text{apparent})$ , calculated in this way, in Figure 10. We note that in the 3 to 5 GeV/c  $P_T$  range the value of  $\sigma_I(\text{apparent})$  thus obtained falls at about the same rate per GeV, a factor of about 25 per GeV, as the single particle cross sections measured by Antreasyan et al.<sup>(23)</sup> We note also that the value of  $\sigma_I(\text{apparent})$  we obtain, at 400 GeV, is about 10 times larger than that reported by Bromberg et al at 200 GeV.<sup>(8)</sup> There are several

$\sigma$  invariant (apparent)  
- see text

FIG. 10

400 GEV  
 $pp \rightarrow \text{jet} + X$

PRELIMINARY RESULTS  
E-395



obvious differences in the measurements which could help explain that difference. (1) The beam energy is different, (2) our calorimeter covers a very substantially larger  $\Delta\Omega$  than theirs, has a fully segmented character rather than strip-type construction; and has a different energy resolution, (3) they have used a magnet in their detector arrangement, with a substantial magnetic "kick" relative to the width of their calorimeter; this improves the energy resolution for charged tracks, but introduces major effects of smeared particle trajectories in determining which particles are swept in or out of the calorimeter.

We do have data also for protons at 200 GeV, not yet analyzed as to cross section; we will report that cross section in the near future. Our CM angular coverage at 200 GeV is quite similar to that at 400 GeV, since we are able to readily move the calorimeter appropriately closer to the target at the lower energy.

10. OBSERVATION OF A PEAK IN THE AWAY-SIDE  $P_T$  DISTRIBUTION.  
STRONG TWO-JET CORRELATIONS.

When we trigger on one arm (either arm), the opposite-side momentum distribution shows a peak. This is a new result. All previous high  $p_T$  experiments that have been reported have in general shown only single-particle momentum spectra on the away side<sup>(25)</sup>. These spectra have regularly shown a monotonic decrease as the single-particle  $p_T$  increases.

With our apparatus, however, we are able to look for possible away-side jets, which might give a  $P_T$  roughly balancing the trigger-side  $P_T$ , and which might thus indicate the occurrence of hard collisions. In fact we do see roughly such an effect.

We proceed as follows. We describe here the case that we trigger with an L trigger. Then in software we select events in various well-defined PT(LEFT) bands. We then examine the PT(AWAY) spectrum--i.e., in this case the PTR spectrum. That spectrum typically shows a broad peak; and the position of the peak increases with the value of the trigger  $P_T$ .

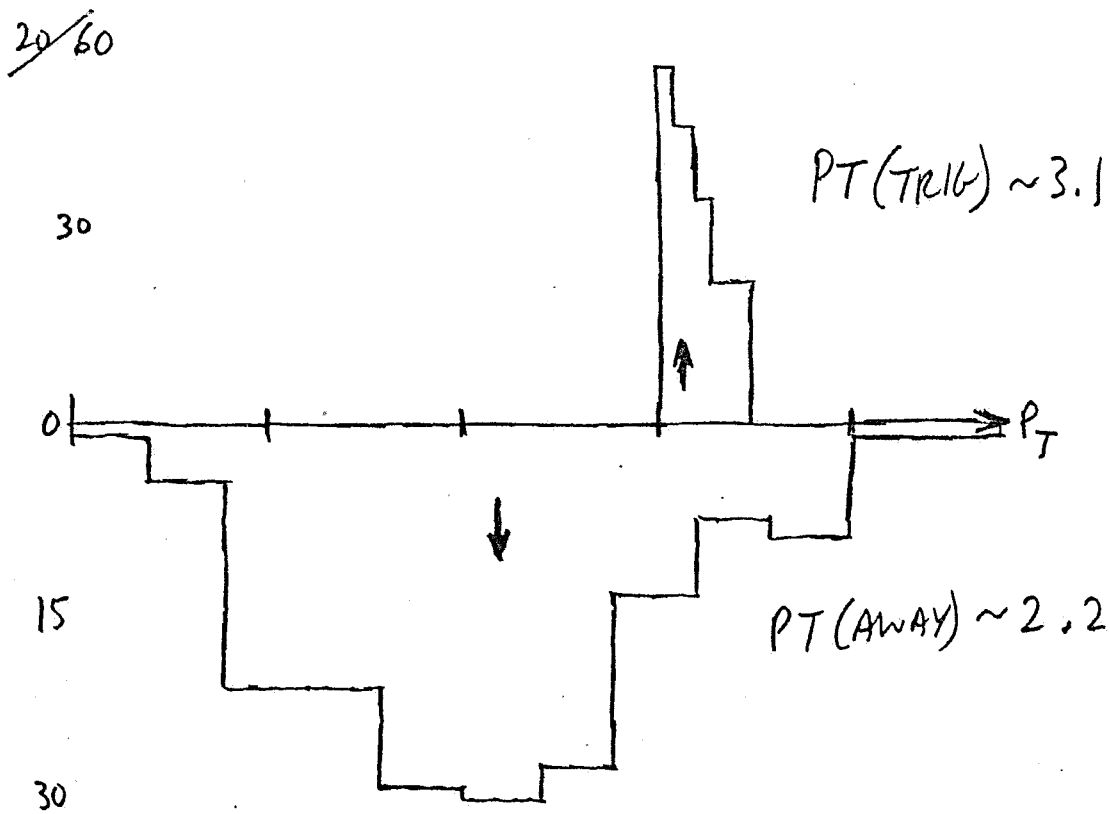
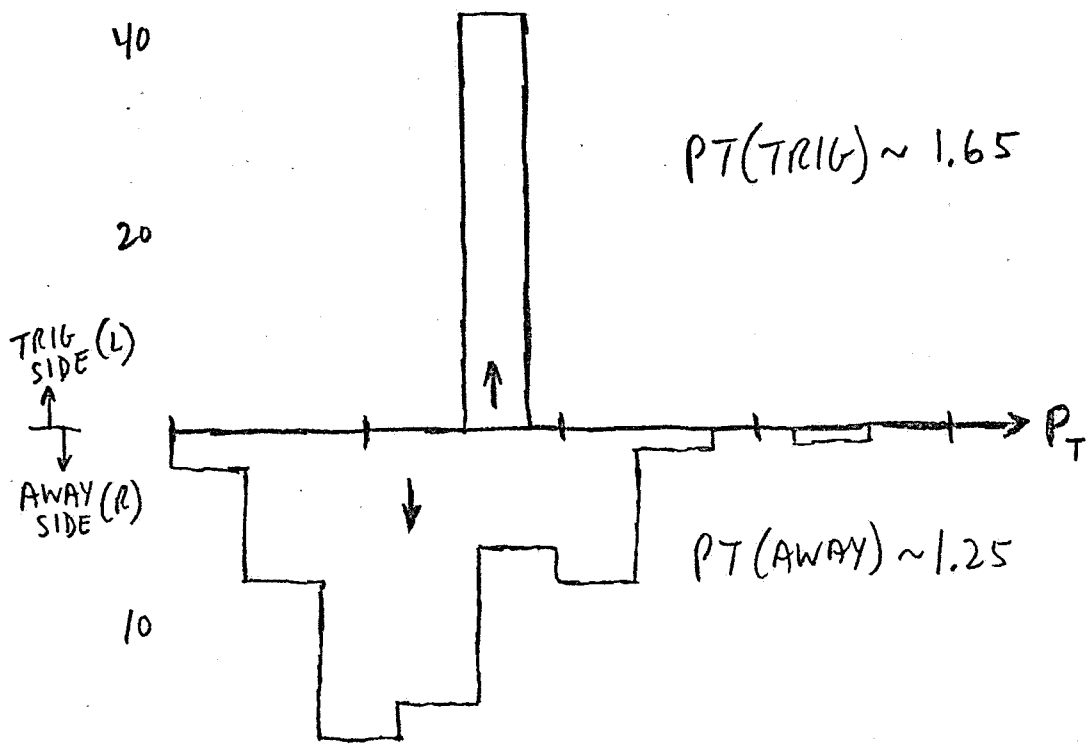
We do not show those spectra here, but instead only the results when we further de-limit the directions of the jet axis on the trigger side and the jet axis on the away side. As discussed in Section 9, there appears to be a region of about 0.1 sr, in the center of each arm, in which the density of events, plotting the direction of the jet axis, is roughly uniform and is about 5 times larger than the density averaged over the entire arm. If we require first of all that the trigger-side jet axis lie in the 0.1 sr fiducial region, then (a) the number of events decreases by about 3, and (b) the peak in the away-side  $P_T$  spectrum moves to a higher value. If we then further require that the jet axis for the AWAY side also lie in the fiducial 0.1 sr for its arm, then the number of events decreases by a further factor, of 2.5 (for higher trigger  $P_T$  values) to 4 (for lower ones). The final result is shown for two sample trigger- $P_T$  bands in Figure 11. The peaking on the AWAY side is clear, and the tendency of the away-side peak to follow the trigger-side  $P_T$  value is also clear.

Figure 12 shows the steady movement of the PT(AWAY) peak with PT(TRIGGER), for a small sample of the data we have taken. We see that (a) as PT(TRIG) increases from 1.5 to 3.5 GeV/c the away-side peak position increases steadily, and (b) in this range the away side peak lies 0.5 to 1.0 GeV/c below the trigger side peak.

This effect must be studied further--we emphasize that this result is a preliminary one. But the away-side peak has shown up from the very first data we have taken, it is present even without making fiducial angle cuts on either side, and it is present whichever arm is used as the trigger arm. We should also emphasize that in the vicinity of such a peak the calorimeter resolution has no significant effect.

Presumably this new observation of an away-side peak occurs only because our away-side detector, as well as the triggering detector, is of calorimeter type and of relatively large solid angle. In fact, since it has long been known that for high  $p_T$  events a rough co-planarity effect exists, the trigger-side fiducial solid angle cut tends to give events with the away-side particles in the plane of the away-side arm--one then requires only adequate  $\theta$ -coverage with that arm (and of course also adequate  $\phi$  coverage to detect those fragments somewhat out of the trigger plane) in order to have a good chance of seeing the opposite

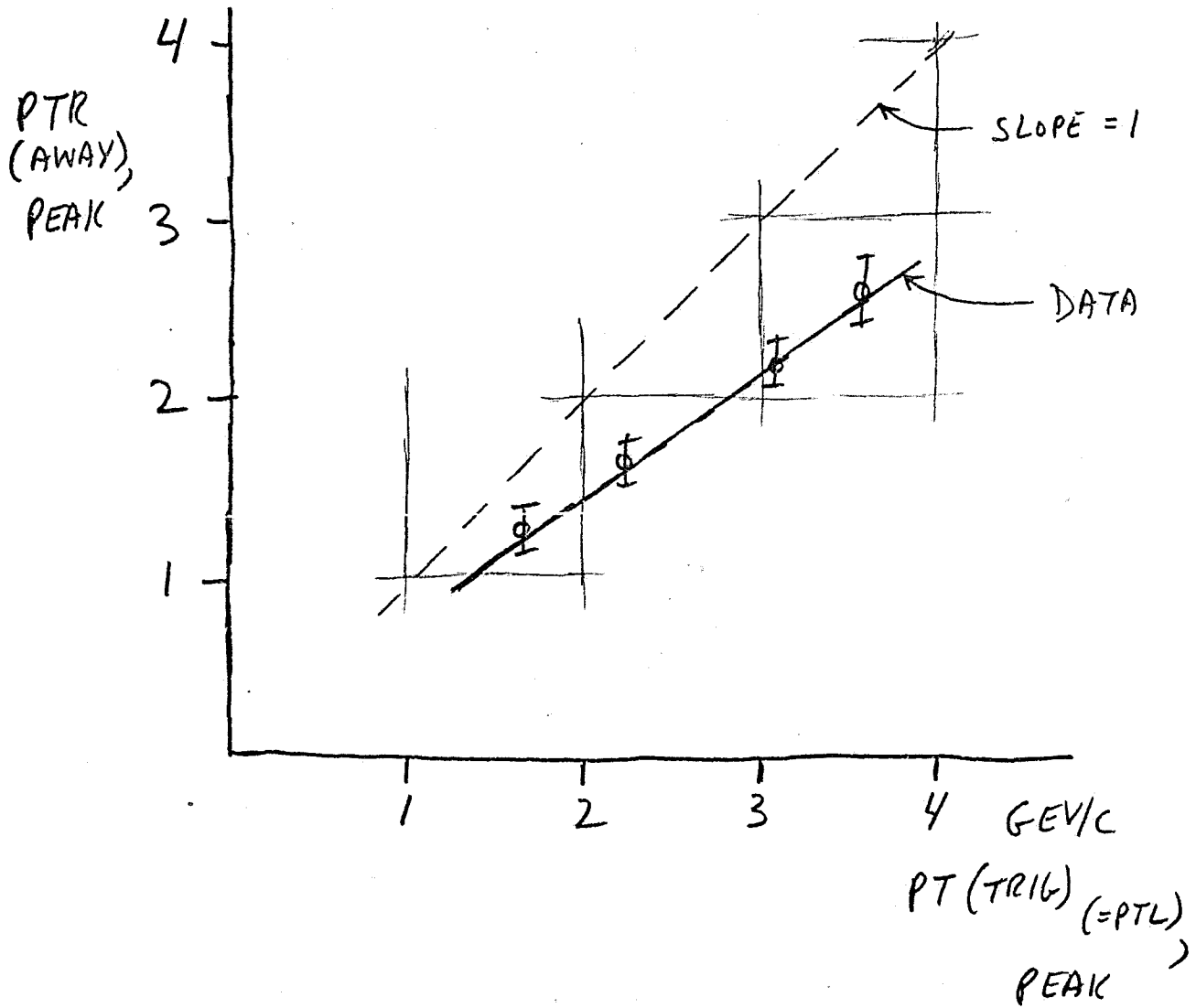
FIG. 11



THE AWAY-SIDE  $P_T$  SPECTRUM FOR TWO  $P_T(\text{TRIG})$  BANDS

FIG. 12

PRELIMINARY RESULTS - E395



PT (AWAY) VS. PT (TRIG),  
CORRELATION

side  $p_T$  , provided that the opposite side  $p_T$  is carried off at large angles rather than, say, along the beam direction. The facts that (1) the opposite side spectrum is so clearly peaked, (2) the two-jet cross section is such a large fraction of the triggering cross section even when the away side jet axis is constrained to lie in a roughly  $20^\circ \times 20^\circ$  interval, and (3) the away-side  $P_T$  follows the trigger-side  $P_T$  value, are all indications of a strongly correlated and closely coplanar two-jet structure in all the high  $P_T$  events we observe--i.e., of the presence of two correlated large angle jets.

Such a correlation has been suggested by parton scattering models. In such a model, the difference in the  $PT(\text{TRIG})$  and  $PT(\text{AWAY})$  values would be interpreted as due to transverse Fermi momentum of the initial partons. The data in Figure 12 are in qualitative agreement with such a picture, with the away-side  $P_T$  regularly smaller than the trigger-side value. But the exact quantitative interpretation of these data to give a numerical value for the quark/parton transverse momentum is complicated by a number of factors, and we do not attempt such an evaluation here. Instead we go on to another method we have used to study both two-arm correlations and quark/parton transverse momentum.

## 11. THE L+R TRIGGER. TWO-JET CORRELATIONS. QUARK/PARTON TRANSVERSE MOMENTUM.

In addition to the single-arm triggers described above, we have used a two-arm-sum trigger (see Section 2), which does not favor either arm. This "L+R" trigger permits us to measure (1) the  $P_T$ -dependence of the cross section, independent of effects due to parton transverse momentum, (2) the nature of two-arm correlations for high  $p_T$  events, and (3) the magnitude of parton transverse momentum.

Figure 13 shows a small sample of data taken with the L+R trigger, with the threshold at  $PTL + PTR > 4$  GeV/c. (These  $P_T$ 's are magnitudes.) This Figure shows that the data, for this trigger, are roughly symmetrical around the diagonal, where  $P_T(L)$  and  $P_T(R)$  are equal, and that the density of events decreases as one moves perpendicularly away from the diagonal, toward either axis. Following the discussion given above in terms of the Fermi momentum of the partons,  $k_T$ , we can calculate the rms parton transverse momentum. We use the deviation  $y$  of each point measured perpendicularly from the diagonal, within some chosen band of fixed  $(PTL + PTR)$ , and calculate  $y_{rms}$  from

$$y_{rms} = \sqrt{\langle y^2 \rangle - \langle y \rangle^2}$$

It can readily be shown that in terms of a parton scattering model  $y_{rms} = \langle k_{Tx} \rangle_{\text{projected}}$  where  $\langle k_{Tx} \rangle$  is the rms/transverse momentum of each of the colliding partons (assumed equal for the two colliding partons).

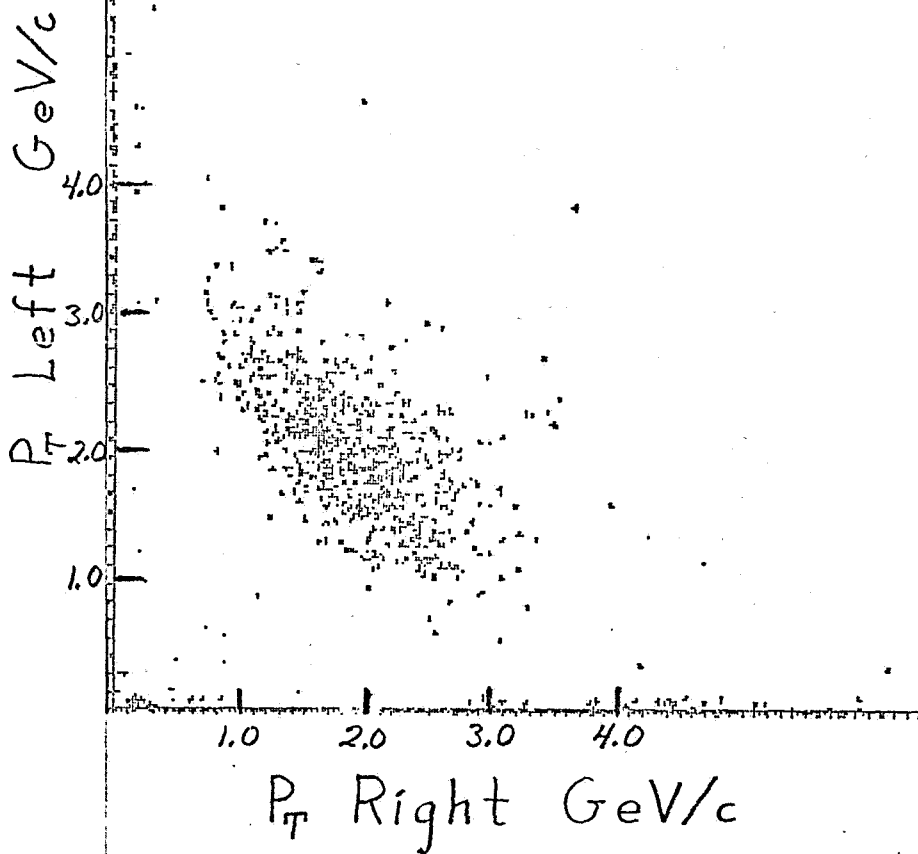
In Figure 14 we show the result of this calculation, for  $(PTL + PTR)/2$  up to about 4.7 GeV/c.

We note that the value of  $\langle k_{Tx} \rangle$  over most of the range in Figure 14, about 0.8 GeV/c, is similar to the value implied for the colliding constituents in the recent dimuon studies of L. Lederman et al. They obtain approximately 1.2 GeV/c<sup>(26)</sup> for  $\langle p_T(\mu\mu) \rangle$ .  $\langle p_T(\mu\mu) \rangle$  is presumably  $\sqrt{2}$  times the individual transverse momentum values of the colliding constituents in that experiment.

We note that the PTL-PTR correlation seen in Figure 13 is quite different from what one would expect in a model using the product of uncorrelated single-arm spectra each corresponding to what has been measured for single

FIG. 13

L+R TRIGGER



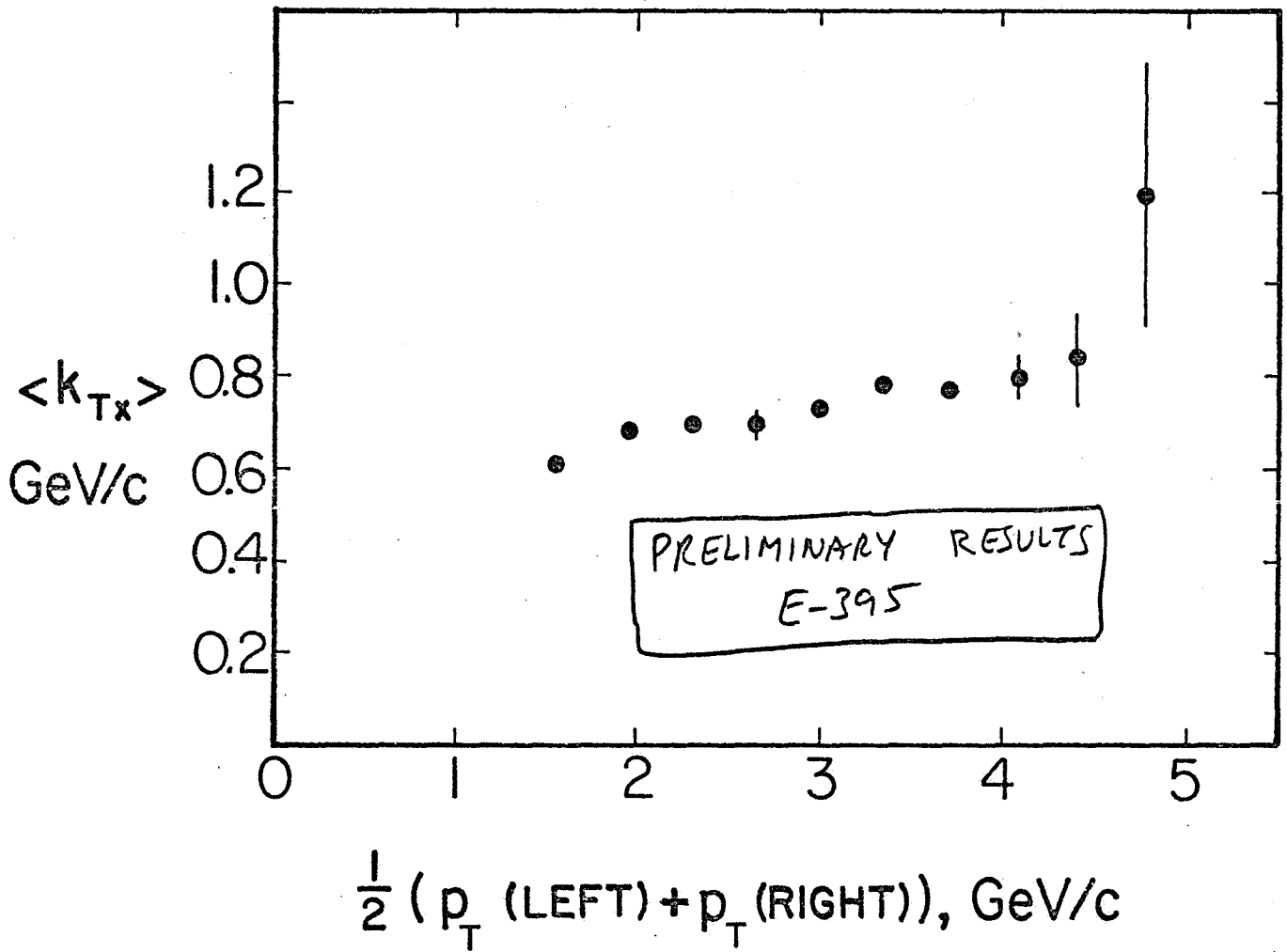


Fig. 14

particles<sup>(23)</sup>. One readily finds that for such an uncorrelated model the regions near the axes would be more densely populated than the region near the diagonal. This is the opposite of what we observe--and that again indicates that we are observing highly correlated high- $p_T$  depositions in the two arms.

## 12. COMPARISON OF JETS PRODUCED BY $\pi^+$ AND PROTON BEAMS

We took data with a positive 200 GeV beam, using the 4 meter position. Incoming  $\pi^+$  and protons were identified by the two double-PM Cerenkov counters in the M2 beam at Fermilab<sup>(27)</sup>. The results of a preliminary analysis of part of our data, examining the production cross section ratio for protons and  $\pi^+$  to make jets with an R trigger, is shown in Figure 15. Analysis of the relative nature of  $\pi^+$  and proton-induced events, including a study of the two-arm angular correlations, is continuing.

## 13. ACKNOWLEDGMENTS,

We are indebted to Fermilab, to ERDA, and to the support groups at Lehigh, Pennsylvania, and Wisconsin, for support and assistance on this work. A great many people have given us particularly important assistance, and we would like to mention specifically M. Atac, F. Codling, T. Droege, T. A. Gabriel, E. L. Goldwasser, M. Hearn, C. Hurlbut, W. Kienzle, R. Shafer, T. Toohig, W. Wales, R. Wardle, G. Widhalm, R. R. Wilson, and E. Worster. Discussions with J. D. Bjorken, M. Jacob, and S. D. Ellis have been invaluable in developing our understanding of this field and our experimental approach.

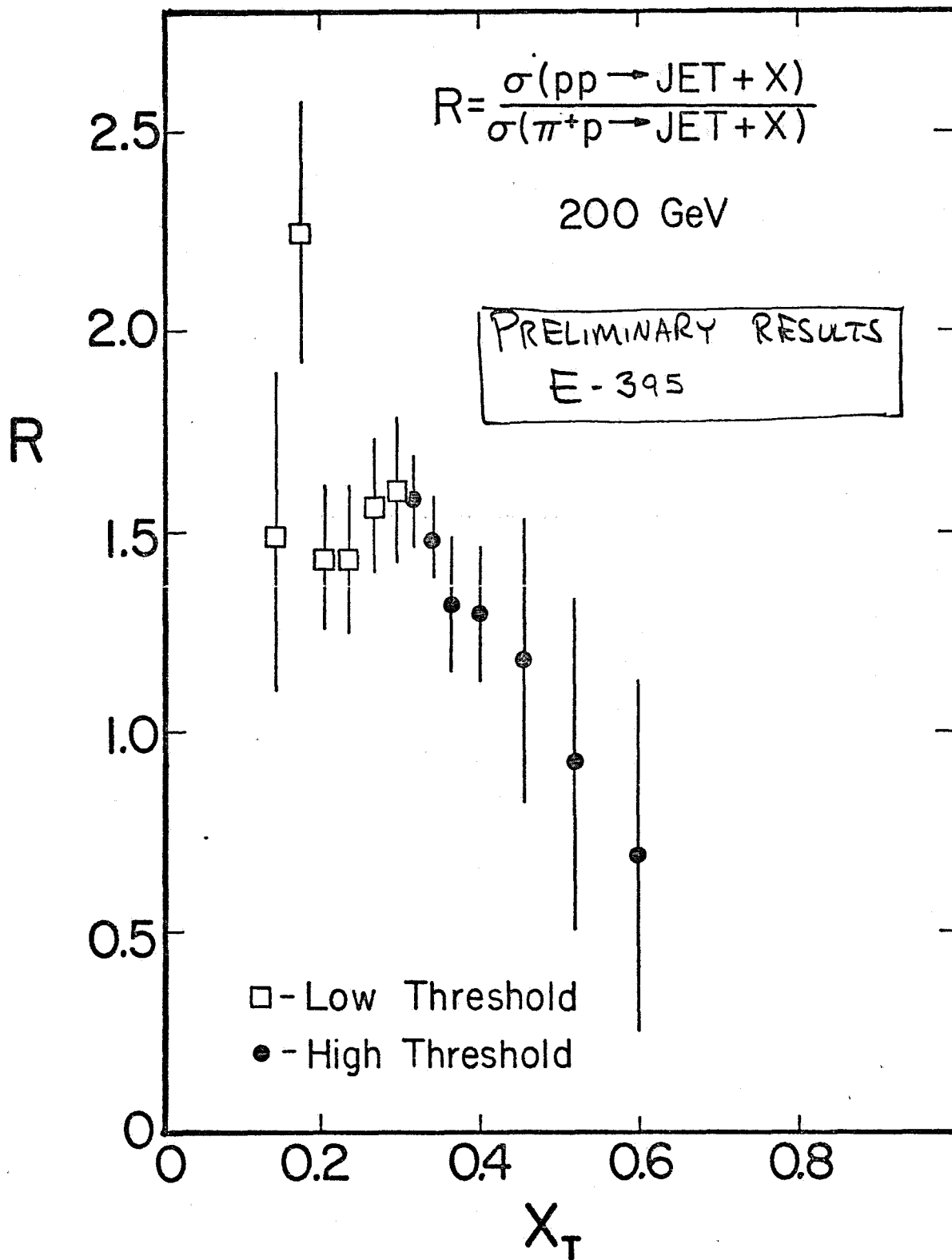


FIGURE 15.

REFERENCES AND FOOTNOTES

1. Berman, Bjorken, and Kogut, Phys. Rev. D4, 3388 (1971).
2. J. D. Bjorken, Phys. Rev. D8, 4098 (1973).
3. See the review article by Sivvers, Brodsky, and Blankenbecler, Physics Reports 23, 1 (1976).
4. P. Darriulat et. al., Nucl. Physics B107, 429 (1976).
5. M. Della Negra et. al., CERN/EP/PHYS 77-10, March 1977 (submitted to Nuclear Physics B).
6. M. Jacob, "Large Transverse Momentum Phenomena", report of ISR Discussion Meeting No. 21, CERN, March 1977 (unpublished); and preceding reports in that series.
7. C. Bromberg et. al., Phys. Rev. Lett. 38, 1447 (1977).
8. C. Bromberg et. al., Fermilab Report Conf-77/62, Aug. 1977 (unpublished).
9. Field and Feynman, Phys. Rev. D15, 2590 (1977).
10. Feynman, Field, and Fox, Caltech report CALT-68-595, 1977 (unpublished).
11. P. V. Landshoff, CERN report TH 2227, Sept. 1976 (unpublished).
12. Ellis and Stroynowski, SLAC report SLAC-PUB-1903, March 1977 (unpublished).
13. ~~Proceedings of the Calorimeter Workshop, M. Atac (Editor), Fermilab, May 1975 (unpublished).~~
14. Developed by W. Kienzle and associates, at CERN, in collaboration with Roehm GmbH, Darmstadt.
15. Obtained from Nuclear Enterprises, Inc., San Carlos, California. We thank Mr. C. Hurlbut for valuable discussions and assistance.
16. We thank Roehm GmbH for assisting us in the preparation of this BBQ-doped acrylic, and for much assistance also in the preparation of other test materials.
17. We thank RCA, Inc., and EMI, Ltd., for undertaking the construction of these special photomultipliers.
18. "Performance of a Sampling Calorimeter at 3 to 17 GeV", BNL-Penn-Wisconsin collaboration, F. Turkot et. al., University of Pennsylvania Internal Report, Oct. 15, 1973 (unpublished). The data are also shown in ref. 19, where they are compared with a theoretical calculation.
19. Gabriel, Amburgey, and Santoro, Nucl. Instr. and Methods 129, 409 (1975).
20. M. Atac et. al., Fermilab report FN-286, January 1976 (unpublished).
21. This system was developed in collaboration with T. Droege of Fermilab.
22. F. W. Busser et. al., Phys. Lett. 46B, 471 (1973).
23. D. Antreasyan et. al., Phys. Rev. Lett. 38, 112 (1977).
24. D. Antreasyan et. al., Phys. Rev. Lett. 38, 115 (1977).

25. See e.g. references 6-8, and reference 3.
26. L. Lederman, private communication.
27. Constructed by R. Walker, A. Tollestrup et. al. We thank H. Haggerty for assistance in the use of these counters (as well as for much other assistance).